

See discussions, stats, and author profiles for this publication at: <https://www.researchgate.net/publication/335082340>

ROS-Responsive Polymeric Nanocarriers with Photoinduced Exposure of Cell-Penetrating Moieties for Specific Intracellular Drug Delivery

Article in *ACS Applied Materials & Interfaces* · August 2019

DOI: 10.1021/acsami.9b10950

CITATIONS

20

READS

1,012

10 authors, including:



Fathy Fathy

University of Science and Technology of China

16 PUBLICATIONS 214 CITATIONS

SEE PROFILE



Wendong Ke

University of Science and Technology of China

33 PUBLICATIONS 1,451 CITATIONS

SEE PROFILE



Jean Felix Mukerabigwi

University of Rwanda

43 PUBLICATIONS 563 CITATIONS

SEE PROFILE



Abd Al-Wali Mohammed M. Japir

University of Science and Technology of China

20 PUBLICATIONS 205 CITATIONS

SEE PROFILE

Some of the authors of this publication are also working on these related projects:



Block copolymer drug delivery for cancer therapy [View project](#)



Nanoreactors as in vivo nanofactories for treatment and diagnosis [View project](#)

ROS-Responsive Polymeric Nanocarriers with Photoinduced Exposure of Cell-Penetrating Moieties for Specific Intracellular Drug Delivery

Fathelrahman Mohammed, Wendong Ke, Jean Felix Mukerabigwi, Abd Al-Wali Mohammed M. Japir, Alhadi Ibrahim, Yuheng Wang, Zengshi Zha, Nannan Lu, Min Zhou, and Zhishen Ge

ACS Appl. Mater. Interfaces, **Just Accepted Manuscript** • DOI: 10.1021/acsami.9b10950 • Publication Date (Web): 09 Aug 2019

Downloaded from pubs.acs.org on August 12, 2019

Just Accepted

“Just Accepted” manuscripts have been peer-reviewed and accepted for publication. They are posted online prior to technical editing, formatting for publication and author proofing. The American Chemical Society provides “Just Accepted” as a service to the research community to expedite the dissemination of scientific material as soon as possible after acceptance. “Just Accepted” manuscripts appear in full in PDF format accompanied by an HTML abstract. “Just Accepted” manuscripts have been fully peer reviewed, but should not be considered the official version of record. They are citable by the Digital Object Identifier (DOI®). “Just Accepted” is an optional service offered to authors. Therefore, the “Just Accepted” Web site may not include all articles that will be published in the journal. After a manuscript is technically edited and formatted, it will be removed from the “Just Accepted” Web site and published as an ASAP article. Note that technical editing may introduce minor changes to the manuscript text and/or graphics which could affect content, and all legal disclaimers and ethical guidelines that apply to the journal pertain. ACS cannot be held responsible for errors or consequences arising from the use of information contained in these “Just Accepted” manuscripts.

1
2
3
4
5
6
7
8
9
10
11
12
13
14
15
16
17
18
19
20
21

ROS-Responsive Polymeric Nanocarriers with Photoinduced Exposure of Cell-Penetrating Moieties for Specific Intracellular Drug Delivery

22 *Fathelrahman Mohammed,^{†,1} Wendong Ke,^{†,1} Jean Felix Mukerabigwi,¹ Abd Al-Wali Mohammed*
23 *M. Japir,¹ Alhadi Ibrahim,¹ Yuheng Wang,¹ Zengshi Zha,¹ Nannan Lu,² Min Zhou,³ and Zhishen*
24 *Ge*.¹*
25
26
27
28
29
30

31 ¹CAS Key Laboratory of Soft Matter Chemistry, Department of Polymer Science and
32 Engineering, University of Science and Technology of China, Hefei 230026, Anhui, China
33

34 ²Department of Oncology, The First Affiliated Hospital of University of Science and Technology
35 of China, Hefei 230001, Anhui, China.
36

37 ³Neurocritical Care Unit, The First Affiliated Hospital of USTC, Division of Life Sciences and
38 Medicine, University of Science and Technology of China, Hefei 230001, Anhui, China.
39
40
41
42
43
44
45
46

47 **KEYWORDS:** ROS-responsive, photodynamic therapy, chemotherapy, drug delivery, cell
48 penetrating
49
50
51
52
53
54
55
56
57
58
59
60

ABSTRACT

In situ modulation of the surface properties on the micellar drug delivery nanocarriers offer an efficient method to improve the drug delivery efficiency into cells while maintaining stealth and stability during blood circulation. Light has been demonstrated to be a temporally and spatially controllable tool to improve cellular internalization of nanoparticles. Herein, we develop reactive oxygen species (ROS)-responsive mixed polymeric micelles with photoinduced exposure of cell-penetrating moieties *via* photodynamic ROS production, which can facilitate cellular internalization of paclitaxel (PTX) and chlorin e6 (Ce6)-coloaded micelles for synergistic effect of photodynamic and chemo-therapy. The thioketal bonds-linked block polymers poly(ϵ -caprolactone)-*TL*-poly(*N,N*-dimethylacrylamide) (PCL-*TL*-PDMA) with a long PDMA block are used to self-assemble into mixed micelles with PCL-*b*-poly(2-guanidinoethyl methacrylate) (PCL-PGEMA) consisting of a short PGEMA block, which are further used to coencapsulate PTX and Ce6. After intravenous injection, prolonged blood circulation of the micelles guarantees high tumor accumulation. Upon irradiation by 660 nm light, ROS production of the micelles by Ce6 induces cleavage of PDMA to expose PGEMA shells for significantly improved cellular internalization. The combination therapy of photodynamic and chemo-therapy inside tumor cells achieves improved antitumor efficacy. The design of ROS-responsive mixed polymeric nanocarriers represents a novel and efficient approach to realize both long blood circulation and high-efficiency cellular internalization for combined photodynamic and chemo-therapy under light irradiation.

INTRODUCTION

Over the past decade, nanomedicine is a promising alternative for diagnosis and treatment of various intractable diseases including cancers.¹⁻³ For efficient delivery of drugs into the target tumor sites *via* systemic administration, there are a variety of physiological barriers that must be overcome for tumor-specific drug delivery through multifunctional properties primarily including long circulation in blood stream with stealthy surfaces, accumulation at the tumor site, uniform distribution inside tumor tissues, and cellular internalization by sticky property for drug release inside cancer cells.⁴ The majority of conventional nanomedicine systems that are approved or in the clinical trials can realize the prolonged blood circulation based on the stealthy tumor accumulation surfaces through well-known permeation and retention (EPR) effect.⁵⁻⁷ Nevertheless, the cellular internalization is often hindered due to the weak interaction between the nanoparticle surfaces and cell membranes, which strictly reduce the final therapeutic efficacy. The most frequently explored strategy is that *in situ* transformation of the surface properties to enhance the cellular uptake of cancer cells in tumor tissues responsive to the internal or external stimuli, such as charge transition from neutral or negative to positive,⁸⁻¹² dePEGylation,¹³⁻¹⁵ and exposure of targeting ligands or cell-penetrating peptide.¹⁶⁻²⁰ Among them, the combination of dePEGylation and exposure of cell-penetrating peptide has shown very high promising potential to maintain high stability of the nanocarriers in blood circulation and achieve very efficient cellular internalization in tumor tissues.^{19,21}

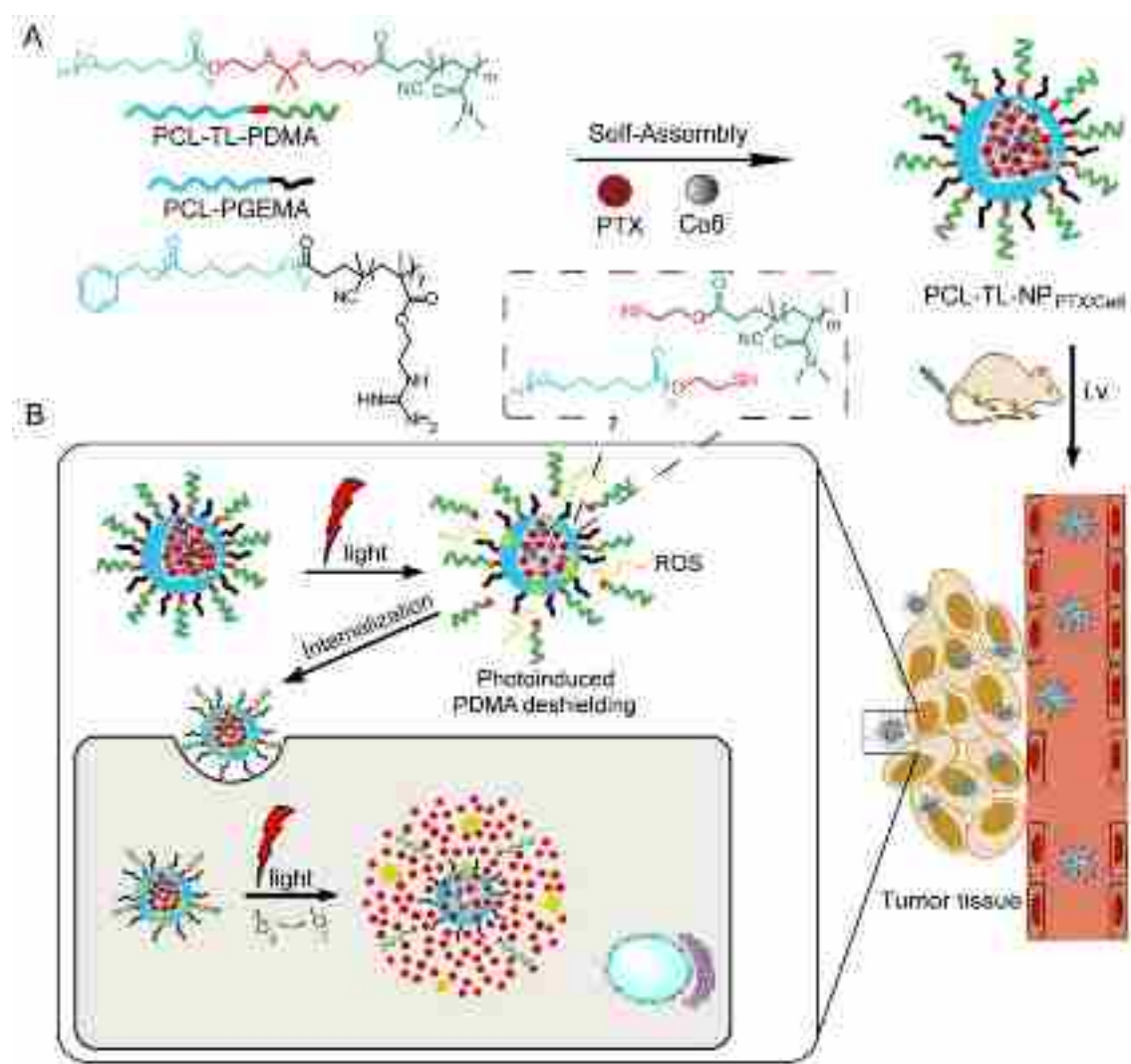
On the other hand, among various stimuli as the trigger of the surface property transition of the nanoparticles, light is especially attractive due to the possibility of high spatio-temporal control.²²⁻²⁴ In particular, the red light or near-infrared light specifically in the wavelength range of 650-950 nm proved greater tissue-penetration depths.²⁵⁻²⁹ Meanwhile, the light can also

1
2
3 perform the photodynamic therapy (PDT) *via* production of reactive oxygen species (ROS) to
4 damage cells.³⁰⁻³² In recent decades, with the development of ROS-responsive materials, the
5 multifunctional nanoparticles to perform PDT were explored to simultaneously release drugs *via*
6 cleavage of ROS-responsive bonds. Notably, thioketal linker (TL) can be readily cleaved by
7 ROS, which was widely used as the ROS-responsive linkage to conjugate drugs or prepare
8 materials.³³⁻³⁸ On the basis of this design, the combination of chemotherapy from the released
9 drugs and PDT can be achieved to significantly improve the final therapeutic efficacy. In
10 addition, PDT-generated ROS-responsive dePEGylation or nanoparticles size shrinkage have
11 likewise been investigated to improve the interactions between nanoparticles and cancer cells for
12 cellular internalization.^{39,40} However, complete ROS-triggered dePEGylation under PDT is
13 difficult, which cannot improve the intracellular drug delivery remarkably, and more efficient
14 strategies are still urgently needed.

15
16
17
18
19
20
21
22
23
24
25
26
27
28
29
30
31 Herein, we constructed the polymeric nanocarriers self-assembled from the TL linked-
32 amphiphilic diblock copolymer poly(-caprolactone)-TL-poly(*N,N*-dimethylacrylamide) (PCL-
33 TL-PDMA) and PCL-*b*-poly(2-guanidinoethyl methacrylate) (PCL-PGEMA) to achieve PDT
34 and PDT ROS-responsive high-efficiency cellular uptake by co-loading the anticancer drug
35 paclitaxel (PTX) and photosensitizer Chlorin e6 (Ce6) (**Scheme 1**). In brief, PTX and Ce6-
36 loaded mixed nanocarriers of PCL-TL-PDMA and PCL-PGEMA (PCL-TL-NP_{PTX/Ce6}) with the
37 coverage of longer hydrophilic PDMA shells for shielding the cellular internalization function of
38 PGEMA to increase systemic circulation half-life and accumulate in tumor tissues through
39 enhancement of EPR effect. PCL-TL-NP_{PTX/Ce6} can produce ROS upon 660 nm red light
40 irradiation at tumor sites, leading to cleavage of the thioketal linkers for exposure of cell-
41 penetrating moieties, PGEMA,⁴¹ which significantly enhances the cellular uptake and
42
43
44
45
46
47
48
49
50
51
52
53
54
55
56
57
58
59
60

subsequently boosts effective drug release. PCL-TL-NP_{PTX/Ce6} nanocarriers were demonstrated to facilitate combination of PDT and chemotherapy *via in vitro* and *in vivo* studies. The designed nanocarriers represent an effective strategy to realize efficient combined PDT and chemotherapy of cancers.

Scheme 1. Schematic illustration for preparation of (A) PTX and Ce6-co-loaded ROS-responsive nanoparticles (PCL-TL-NP_{PTX/Ce6}), (B) mechanism of ROS-responsive cleavage of PDMA to improve the cellular uptake upon 660 nm red light irradiation; and synergistic effect of PDT and chemotherapy through high-efficiency cellular uptake and drug release.



EXPERIMENTAL PROCEDURES

Materials. Dicyclohexylcarbodiimide (DCC, 98%), azobisisobutyronitrile (AIBN, 99%), 4-dimethylaminopyridine (DMAP, 98%), tin 2-ethylhexanoate ($\text{Sn}(\text{Oct})_2$), and 9, 10-diphenylanthracene DPA were procured from Sigma-Aldrich. N, N-Dimethylacrylamide was purchased from Aldrich and purified through distillation under vacuum. ϵ -Caprolactone (CL) and Toluene were dried over calcium hydride CaH_2 and collected by distilled under vacuum before use. PTX (98%) was supplied by Jiangyuan Natural Products Co. Ltd. Ce6 (98%) was bought from J&K Scientific Ltd and used as received. Fetal bovine serum (FBS), Phosphate-buffered saline (PBS), Dulbecco's modified Eagle's medium (DMEM), trypsin, 3-(4, 5-dimethyl-2-thiazolyl)-2, 5-diphenyl-tetrazolium bromide (MTT), and 4, 6-diamidino-2-phenylindole (DAPI) were provided by Beyotime Institute of Biotechnology (Shanghai, China). 2,2'-(Propane-2,2-diylbis(sulfanediy))bis(ethan-1-ol) (TL),^{32,42} 4-cyano-4-(2-phenylethane sulfanylthiocarbonyl) sulfanyl pentanoic acid (PETTC),⁴³ PCL-based macro RAFT agent (PCL-RAFT),⁴⁴ and 2-guanidinoethyl methacrylate (GEMA)⁴¹ were synthesized as previously reported procedures. The human cervical cancer cell line HeLa and cell line H22 of murine hepatic carcinoma were kindly provided by Chinese Academy of Sciences Cell Bank (Shanghai, China). Female BALB/c mice at the age of 5-Week were obtained from Vital River Lab Animal Technology Co., Ltd. The animal experiments were conducted in accordance with the Experimental Animals Administration Regulations (Hefei, revised in June 2013).

1
2
3 **Synthesis of PCL-TL-PDMA.** The synthetic routes to prepare block copolymers, PCL-TL-
4 PDM, PCL-PDMA, and PCL-PGEMA, are illustrated in **Scheme S1** and the methods are
5 described as follows.
6
7

8
9
10 **Synthesis of thioketal linker-containing RAFT agent (RAFT-TL).** TL (0.235 g, 1.2 mmol),
11 DMAP (0.012 g, 0.09 mmol), and DCC (0.20 g, 0.9 mmol) were dissolved in 5 mL of anhydrous
12 (DCM) and stirred under nitrogen atmosphere at 25 °C for 30 min. PETTC (0.34 g, 1 mmol) in
13 5 mL anhydrous DCM was then added dropwise to the mixture and allowed to react overnight
14 under stirring at 25 °C. Finally, DCM was removed from the resulting product under vacuum ,
15 then purified by silica column chromatography eluted by (ethyl acetate: petroleum ether, 2:3 v/v)
16 to obtain the pure product as yellowish oily paste (0.45 g, yield: 81%). ¹H NMR (**Figure 1A**, 300
17 MHz, CDCl₃), (ppm): 7.35 (m, 2H), 7.24 (d, *J* = 1.6 Hz, 2H), 4.28 (t, *J* = 6.9 Hz, 2H), 3.79 (t, *J*
18 = 6.1 Hz, 2H), 3.60-3.54 (m, 2H), 2.99 (d, *J* = 6.9 Hz, 2H), 2.88 (d, *J* = 6.5 Hz, 4H), 2.68 – 2.62
19 (m, 2H), 2.58-2.49 (m, 1H), 2.42-2.34 (m, 1H), 1.89 (s, 3H), 1.63 (s, 6H). ¹³C NMR (CDCl₃),
20 (ppm): 216.52 , 171.30, 139.18, 128.59, 61.50 , 37.97 , 34.07, 33.73, 31.13, 29.71, 29.03, 24.86.
21 (ESI-MS): Calculated: [C₂₂H₃₂O₃NS₅] 518.097, found: 518.098 (**Figures S1 and S2**).
22
23
24
25
26
27
28
29
30
31
32
33
34
35
36
37
38

39 **Synthesis of TL-containing PDMA macroRAFT agent (PDMA-RAFT-TL).** RAFT-TL (52
40 mg, 0.1 mmol), AIBN (1.8 mg, 0.011 mmol), and DMA (0.72 g, 7.3 mmol) were dissolved in
41 1,4-dioxane (2 mL) and added to 5 mL Schlenk flask. After degassing by three freeze-pump-
42 thaw cycles, the flask was sealed under vacuum. Then the polymerization was conducted into an
43 oil bath at 70 °C for 12 h under moderate stirring. Thereafter, the reaction tube was immersed
44 into liquid nitrogen to stop the polymerization, followed by precipitation into cold diethyl ether
45 and dissolve in DCM and then precipitate again in ether for 2 more times. The final product was
46 dried in a vacuum oven to obtain a yellow solid compound (0.59 g, yield: 78%, *M_n*, GPC = 7100,
47
48
49
50
51
52
53
54
55
56
57
58
59
60

1
2
3 $M_w/M_n = 1.13$). The degree of polymerization (DP) of PDMA segment was determined to be 72
4 based on the ^1H NMR analysis in CDCl_3 (**Figure S3**), the obtained polymer was mentioned as
5
6 PDMA₇₂-RAFT-TL.
7
8
9

10
11 **Synthesis of PCL-TL-PDMA.** PDMA₇₂-RAFT-TL (0.22 g, 0.029 mmol), CL (0.46 g, 4.1
12 mmol), and Sn (Oct)₂ (0.015 mmol) dissolved in dry toluene (3 mL), were introduced into
13 flamed Schlenk flask equipped with a Teflon coated magnetic stir bar. After evaporation of ~ 0.5
14 mL, the flask was then degassed by three freeze–pump–thaw cycles. The flask was flame sealed
15 under vacuum then placed in a thermostatted oil bath at 120 °C to initiate the polymerization.
16 After 12 h of polymerization, the resulting product was diluted by DCM and added dropwise into
17 excess cold diethyl ether for precipitation. Thereafter, the residues were redissolved again in
18 DCM and repeat precipitation two times in ether. Finally, the final product was dried in a
19 vacuum oven to obtain a yellowish solid powder (0.52 g, yield: 77%, $M_n = 19200$, $M_w/M_n =$
20 1.20). The actual DP of PCL segment was determined to be 135 by ^1H NMR analysis in CDCl_3
21 (**Figure 1B**). Thus, the copolymer was termed as PCL₁₃₅-TL-PDMA₇₂.
22
23
24
25
26
27
28
29
30
31
32
33
34
35
36

37 **Synthesis of PCL-PDMA.** PCL-PDMA was synthesized by using PCL₁₃₇-RAFT as the chain
38 transfer agent. Briefly, PCL₁₃₇-RAFT (0.44 g, 0.028 mmol), DMA (0.207 g, 2.1 mmol), and
39 AIBN (0.5 mg, 0.003 mmol) were dissolved in 1,4-dioxane (2 mL) and poured into to flamed
40 flask. Then the flask was degassed by three freeze-pump-thaw cycles and sealed under vacuum.
41 The polymerization was initiated after immersion into an oil bath at 80 °C. After 18 h of
42 polymerization, the resulting product was diluted by DCM and added dropwise into excess cold
43 diethyl ether for precipitation. Thereafter, the product was redissolved again in DCM and repeat
44 precipitation two times in ether. Finally, the product was dried in a vacuum oven to obtain faint
45 yellow product (0.53 g, yield: 81%, $M_{n, \text{GPC}} = 18,022$, $M_w/M_n = 1.28$). DP of PDMA segment was
46
47
48
49
50
51
52
53
54
55
56
57
58
59
60

1
2
3 calculated to be 70 by ^1H NMR analysis in CDCl_3 (**Figure 1C**). Thus, the copolymer was named
4 as $\text{PCL}_{137}\text{-PDMA}_{70}$. According to the similar procedure, block copolymer PCL-PGEMA was
5 also synthesized ($M_n = 14,200$, $M_w/M_n = 1.24$). The modification of the procedure is changing
6 the solvent for the polymerization in DMSO. DP of PGEMA segment was calculated to be 38
7 according to the ^1H NMR analysis in $\text{DMSO-}d_6$ (**Figure 1D**).
8
9
10
11
12
13
14

Preparation of PTX and Ce6-loaded micellar nanoparticles. The nanoprecipitation method
15 was used to prepare PTX and Ce6-loaded nanocarriers ($\text{PCL-TL-NP}_{\text{PTX/Ce6}}$). Briefly, PTX (1
16 mg), and Ce6 (0.5 mg), PCL-TL-PDMA (5.0 mg), and PCL-PGEMA (2.0 mg) dissolved in
17 DMSO (1.0 mL) were charged into 10 mL vial, followed by quickly adding PBS (9 mL, pH 7.4)
18 under vigorous stirring. The mixture was further stirring for 2 h, and then the mixture solution
19 was subjected to dialysis by using dialysis bag (MWCO, 3500 Da) against PBS for 24 h to
20 remove DMSO. The unencapsulated PTX and Ce6 were removed through a $0.45\ \mu\text{m}$ Millipore
21 filters. The drug loading capacities (DLCs) and drug loading efficiencies (DLEs) were
22 determined according the equations: $\text{DLCs (\%)} = [(\text{wt of loaded drug}) / (\text{wt of total nanocarriers})]$
23 $\times 100$. $\text{DLEs (\%)} = [(\text{wt of loaded drug in nanocarriers}) / (\text{wt of total drug in feed})] \times 100$. DLCs
24 of PTX and Ce6 in $\text{PCL-TL-NP}_{\text{PTX/Ce6}}$ were determined to be $6.8 \pm 0.31\%$ and 3.3 ± 0.01 ,
25 respectively. As controls, $\text{PCL-NP}_{\text{PTX/Ce6}}$ with DLC of PTX and Ce6 $6.6 \pm 0.26\%$ and $3.2 \pm$
26 0.89% , respectively, was prepared from the mixture of PCL-PDMA and PCL-PGEMA according
27 to the similar procedure. Only Ce6-loaded PCL-TL-PDMA nanoparticles $\text{PCL-TL-NP}_{\text{Ce6}}$ were
28 prepared with Ce6 DLC of $3.6 \pm 0.11\%$.
29
30
31
32
33
34
35
36
37
38
39
40
41
42
43
44
45
46
47
48
49
50

Detection of singlet oxygen production. Singlet oxygen production from $\text{PCL-TL-NP}_{\text{PTX/Ce6}}$
51 under light irradiation was detected by DPA.⁴⁵ Briefly, $\text{PCL-TL-NP}_{\text{PTX/Ce6}}$ (200 μL , 1 mg/mL)
52 was mixed with 20 μM DPA. Subsequently, the solution was irradiated by 660 nm red light at a
53
54
55
56
57
58
59
60

1
2
3 power density of 80 mW/cm² for different times. The fluorescence intensity of DPA at 400 nm
4 was recorded. The generation of singlet oxygen by PCL-TL-NP_{PTX/Ce6} can bleach DPA, thus, the
5 reduction in DPA absorption at 400 nm was reflects the singlet oxygen level produced by PCL-
6 TL-NP_{PTX/Ce6} .and the nanoparticle solution without light irradiation was used as the control.
7
8
9

10
11
12
13 **Degradation of PCL-TL-NP_{Ce6} under light.** PCL-TL-NP_{Ce6} (1 mg/mL, 10 mL) solution in a
14 transparent tube was suspended in PBS at 37 °C, then exposed to 660 nm red light for a
15 predetermined time (0, 20, 40, 60, 80, 100, and 120 min). Subsequently, the nanoparticles
16 solutions were gathered and lyophilized for GPC analysis.
17
18
19

20
21
22
23 **Drug release.** PTX release profiles from PCL-TL-NP_{PTX/Ce6} and PCL-NP_{PTX/Ce6} were studied
24 with or without light irradiation. Typically, freshly prepared PCL-TL-NP_{PTX/Ce6} and PCL-
25 NP_{PTX/Ce6} (1.0 mL) were first irradiated for 40 min under irradiation of 660 nm red light at power
26 density of 80 mW/cm². Subsequently, the solutions were subjected into the dialysis membranes
27 and then incubated into PBS (5 mL, pH 7.4, 10 mM) at 37 °C with slow shaking (90 rpm). At
28 different time intervals, the releasing media (1 mL) was replaced with 1 mL fresh media. The
29 released amount of PTX was measured by using High-performance liquid chromatography
30 (HPLC) analysis (mobile phase: acetonitrile/H₂O (3:7, v/v).
31
32
33
34
35
36
37
38
39
40
41

42
43 **Cellular uptake of PCL-TL-NP_{PTX/Ce6}.** Cellular uptake of PCL-NP_{PTX/Ce6} and PCL-TL-
44 NP_{PTX/Ce6} in HeLa cells was quantitatively detected using flow cytometry and CLSM. For flow
45 cytometry analysis, HeLa cells were cultured into 12-well plates at 37 °C at a density of 5 × 10⁴
46 cells per well in medium (500 μL) at 37 °C in 5% CO₂ humidified atmosphere containing 10%
47 FBS and incubated for 24 h .Then the DMEM medium was removed and replaced by (500 μL)
48 fresh medium containing PBS, PCL-NP_{PTX/Ce6}, and PCL-TL-NP_{PTX/Ce6} at ([PTX] = 4.0 μg/mL
49
50
51
52
53
54
55
56
57
58
59
60

1
2
3 and [Ce6] = 1.94 $\mu\text{g/mL}$) this ratio is fixed as the PCL-TL-NP_{PTX/Ce6} nanoparticle was prepared.
4
5 After incubation for 4 h, the cells were subsequently irradiated by 660 nm light (80 mW/cm²) for
6
7 40 min and the cells without light irradiation were used as control. Thereafter further incubation
8
9 for 2 h, the cells were digested, collected, and then suspended in PBS to be measured by flow
10
11 cytometer.
12
13

14 For CLSM observation, HeLa cells were incubated with PCL-NP_{PTX/Ce6} and PCL-TL-
15
16 NP_{PTX/Ce6} at ([PTX] = 4.0 $\mu\text{g/mL}$ and [Ce6] = 1.94 $\mu\text{g/mL}$) this ratio is fixed as the PCL-TL-
17
18 NP_{PTX/Ce6} nanoparticle was prepared. After incubation for 4 h, the cells were irradiated by 660
19
20 nm light (80 mW/cm²) for 40 min and the cells without light irradiation were used as control.
21
22 After further incubation for 2 h, subsequently, the cells were washed with PBS, and the cell
23
24 nuclei were stained with DAPI for 15 min, followed by washing with PBS to remove free DAPI,
25
26 and imaging by CLSM.
27
28
29

30 Additionally, to detected the intracellular ROS production from PCL-TL-NP_{PTX/Ce6}, HeLa cell
31
32 line were cultured in 24-well plates at 37 °C at a density of 1×10^5 cells per well in DMEM (500
33
34 μL) at 37 °C in 5% CO₂ humidified atmosphere containing 10% FBS. After 24 h incubation for,
35
36 the medium was removed and add fresh medium (500 μL) containing PBS, free Ce6, PCL-TL-
37
38 NP_{PTX/Ce6}, and PCL-NP_{PTX/Ce6} and incubated for 24 h at ([PTX] = 4.0 $\mu\text{g/mL}$ and [Ce6] = 1.94
39
40 $\mu\text{g/mL}$) this ratio is fixed as the PCL-TL-NP_{PTX/Ce6} nanoparticle was prepared. Then the ROS
41
42 detection reagent DCFH-DA (10 μM) was added and incubated for 30 min followed by light
43
44 irradiation for 40 min. Finally, the green fluorescence of oxidized DCFH-DA that can indicate
45
46 the intracellular ROS levels was monitored using fluorescence microscope and flow cytometer.
47
48
49

50
51
52 ***In vitro* cytotoxicity.** HeLa cells were seeded into 96-well plates at a density of 1×10^4 cells per
53
54 well in (100 μL) of DMEM at 37 °C in 5% CO₂ humidified atmosphere containing 10% FBS.
55
56
57
58
59
60

After incubation for 24 h, the medium was removed and add fresh medium containing free PTX/Ce6, PCL-TL-NP_{Ce6}, PCL-TL-NP_{PTX}, PCL-TL-NP_{PTX/Ce6}, and PCL-NP_{PTX/Ce6} at various concentrations. Following incubation for 4 h, then the partial groups were irradiated with red light irradiated for 40 min. All the groups were subsequently incubated at 37 °C for another 44 h. Therefore, the cell viability was determined by MTT assays. Briefly, MTT probe dissolved in PBS (20 μL, 5 mg mL⁻¹) was added to each well and further incubate for 4 h at 37 °C in the dark. Next, the medium was removed and replaced by 200 μL of DMSO, and then the culture plate was subjected to shaking for 30 min under dark environment to dissolve the formed purple formazan crystals. Finally, the cell cytotoxicity was evaluated based on the recorded absorbance intensity by microplate reader at 490 nm. Moreover, the values of half maximum inhibitory levels (IC₅₀) were calculated using MTT results by GraphPad Prism software. The synergy between PTX and Ce6, the combination index (CI) of their IC₅₀ values was calculated according to Chou-Talalay's isobolographic method,⁴⁶ we also calculated the PTX and Ce6 combined index (CI) values of PCL-TL-NP nanocarriers. The Equation (1) was described as follows, and the CI value (CI >1), additively (CI = 1), or synergism (CI <1), respectively. Equation 1:

$$CI = \frac{C_{\text{PCL-TL-NP@PTX/Ce6}}}{C_{\text{PTX}}} + \frac{C_{\text{PCL-TL-NP@PTX/Ce6}}}{C_{\text{Ce6}}} + \frac{(C_{\text{PCL-TL-NP@PTX/Ce6}})(C_{\text{PCL-TL-NP@PTX/Ce6}})}{(C_{\text{PTX}})(C_{\text{Ce6}})}$$

For cell live/dead studies, HeLa cells were cultured in 24-well at a density of 5×10^4 cells per well in medium (500 μL) at 37 °C with 5% CO₂ humidified atmosphere contained 10% FBS. After 24 h of incubation, the DMEM medium was removed and add fresh medium which contained PBS, PCL-NP_{PTX/Ce6}, and PCL-TL-NP_{PTX/Ce6} at ([PTX] = 4.0 μg/mL and [Ce6] = 1.94 μg/mL) this ratio is fixed as the PCL-TL-NP_{PTX/Ce6} nanoparticle was prepared. After incubated for 4 h, the cells were irradiated for 40 min by 660 nm light at the power of 80 mW/cm². After

1
2
3 20 h of incubation, the medium was completely removed and added PBS (100 μL) in each well.
4
5 Next, FDA solution in DMSO (1 μL , 1 mg mL^{-1}) was then added to each well and subjected to
6
7 further incubation of 20 min at 37 $^{\circ}\text{C}$ in the dark to stain live cells. Subsequently, the medium
8
9 was aspirated and twice washed with PBS followed by adding 100 μL PBS PI solution in DMSO
10
11 (2 μL , 1 mg mL^{-1}) and subjected to further incubation of another 10 min to staining dead cells.
12
13 Then each well was washed twice with fresh PBS and the fluorescence microscopy images were
14
15 obtained.
16
17

18
19 For evaluation of the cell apoptosis, HeLa cells were cultured in 6-well plates at 37 $^{\circ}\text{C}$ at a
20
21 density of 1×10^5 cells per well in DMEM (500 μL) at 37 $^{\circ}\text{C}$ containing 10% FBS. After 24 h of
22
23 incubation, the medium was changed with fresh DMEM containing PBS, PCL-NP_{PTX/Ce6}, and
24
25 PCL-TL-NP_{PTX/Ce6} at ([PTX] = 4.0 $\mu\text{g/mL}$ and [Ce6] = 1.94 $\mu\text{g/mL}$), this ratio is fixed as the
26
27 PCL-TL-NP_{PTX/Ce6} nanoparticle was prepared. Next, the cells were subjected to irradiation with
28
29 660 nm light (80 mW/cm^2) for 40 min after 4 h of incubation. As control the cells incubated with
30
31 PCL-NP_{PTX/Ce6}, and PCL-TL-NP_{PTX/Ce6} were used without light irradiation. After further
32
33 incubation for 20 h, the cells were washed by cold PBS three times, digested, collected and
34
35 stained with Annexin V/PI according to the manufacturer's procedure. Finally the apoptosis
36
37 evaluation was performed by flow cytometric. FlowJo software was utilized to analyze the data.
38
39
40
41
42

43 **Animal tumor model.** To establish the subcutaneous xenograft tumor models, H22 cells ($1.5 \times$
44
45 10^6) were administered by subcutaneous injection into the right flanks of the mice. To evaluate *in*
46
47 *vivo* biodistribution by optical imaging, the mice bearing H22 tumors ($\sim 60 \text{ mm}^3$) were used for
48
49 intravenously injection *via* tail vein with 200 μL of PCL-TL-NP_{PTX/Ce6} or PCL-NP_{PTX/Ce6} at a
50
51 PTX equivalent dose of 10 mg/kg and Ce6 dose of 4.85 mg/kg , this ratio is fixed as the PCL-TL-
52
53 NP_{PTX/Ce6} nanoparticle was prepared. The mice were anesthetized and observed *via* the IVIS *in*
54
55
56
57
58
59
60

1
2
3 *in vivo* Imaging System at 1, 6, 12, 24, and 48 h after injection. Moreover for the tissue
4 nanoparticles distribution study, the treated mice at 48 h after injection were sacrificed. The main
5 organs were collected for IVIS observation including the heart, liver, spleen, lung, kidney, and
6 tumor.
7
8
9
10

11
12
13 **Pharmacokinetics and biodistribution.** Free PTX, PCL-NP_{PTX/Ce6}, and PCL-TL-NP_{PTX/Ce6} (200
14 μ L) at a PTX equivalent dose of 10 mg/kg were intravenously administrated to BALB/c mice
15 bearing H22 tumors. At given time intervals, blood samples from the retro-orbital mouse eyes
16 plexus were collected, and then was extracted with chloroform/acetonitrile (1.0 mL, 4:1, v/v) on
17 a vortex for 5 min. The samples were then centrifuged at $10,000 \times g$ for 10 min. Finally, HPLC
18 analysis was used to measure the PTX concentration in the supernatant.
19
20
21
22
23
24
25
26

27 To evaluate the biodistribution of the drugs in varying organs, mice bearing H22 tumors were
28 intravenously injected by free PTX, PCL-NP_{PTX/Ce6}, and PCL-TL-NP_{PTX/Ce6} at the injection
29 dosages of PTX 10 mg/kg. Thereafter, the main organs and tumor tissues at 48 h post-injection
30 were harvested, weighted, and homogenized in PBS. PTX was extracted with
31 chloroform/acetonitrile (4:1, v/v) and the solutions were centrifuged at 4 °C (3000 g, 10 min).
32 The resulting solvents were evaporated under reduced pressure and the HPLC analysis quantified
33 the PTX concentration by using acetonitrile/H₂O (3:7, v/v) as the elution solvent.
34
35
36
37
38
39
40
41
42
43

44 **ROS production in tumor tissues.** In order to evaluate the production of ROS in tumors using a
45 DCFH-DA fluorescence probe, the mice bearing H22 tumors ($\sim 60 \text{ mm}^3$) were injected
46 intravenously with free Ce6, PCL-TL-NP_{PTX/Ce6}, and PCL-NP_{PTX/Ce6} (200 μ L) at the PTX
47 equivalent dose of 10 mg/kg and Ce6 dose of 4.85 mg/kg, this ratio is fixed as the PCL-TL-
48 NP_{PTX/Ce6} nanoparticle was prepared. After 24 h post-injection, the tumors were injected
49 intratumorally with (50 μ L, 25 μ M) DCFH-DA probe, then irradiated with red light (80
50
51
52
53
54
55
56
57
58
59
60

mW/cm², 660 nm) for 40 min. The mice were sacrificed after 30 min, and the tumors were collected for CLSM observation and sectioned into 10 μm thick slices.

***In vivo* antitumor efficacy.** When H22 tumors reached ~ 60 mm³, the mice bearing H22 tumors were spontaneously divided into 7 groups (PBS, free PTX, free Ce6, PCL-TL-NP_{PTX/Ce6}, PCL-NP_{PTX/Ce6}) at the PTX equivalent dose of 2.5 mg/kg and Ce6 dose of 1.21 mg/kg. The samples (200 μL) were intravenously injected at day 1, 3, and 5, respectively, this ratio is fixed as the PCL-TL-NP_{PTX/Ce6} nanoparticle was prepared. After 24 h post injection, Ce6, PCL-NP_{PTX/Ce6}, and PCL-TL-NP_{PTX/Ce6} groups received light irradiation (40 min, 660 nm, 80 mW/cm²), and without light irradiation were used as controls. Besides, the tumor growth rate was monitored by measuring the perpendicular diameter using calipers, and volume of the individual tumor was calculated by the following equation: tumor volume = (length × width²)/2. At the end of the treatment, the mice were sacrificed, and the major organs (heart, liver, spleen, lung, and kidney) and tumors were excised for histological examination by standard the hematoxylin and eosin (H&E) staining.

Statistical analysis. All the data were provided as the mean ± SD. Assignments to treatments and selections of fields of microscopic inspection were produced at random. The statistical significance of distinct groups was evaluated using a Student's t-test and in all analysis the p values < 0.05 were considered statistically significant.

RESULTS AND DISCUSSION

Polymers synthesis and nanoparticle preparation. We designed two block copolymers for nanoparticle preparation, the TL-linked amphiphilic diblock copolymer, PCL-TL-PDMA, with a longer chain of PDMA as the hydrophilic segment, and the block copolymer, PCL-PGEMA,

1
2
3 with a relatively shorter PGEMA chain (**Scheme S1**). To prepare the block copolymer, PCL-TL-
4 PDMA, TL was first reacted with PETTC *via* esterification reaction to obtain RAFT-TL. The
5 preparation of RAFT-TL was fully characterized by ^1H NMR, ^{13}C NMR, and ESI-MS (**Figures**
6 **1A, S1, and S2**). RAFT-TL was used as the RAFT agent to polymerize DMA monomer for the
7 synthesis of PDMA-RAFT-TL with DP of 72 as showed by ^1H NMR analysis and distribution of
8 low molecular weight ($M_w/M_n = 1.13$) as evidenced by gel permeation chromatography (GPC)
9 analysis (**Figures 1E and S3**). Subsequently, PDMA-RAFT-TL was used as ring-opening
10 polymerization (ROP) macro-initiator of CL by using of $\text{Sn}(\text{Oct})_2$ as the catalyst. The block
11 copolymer, PCL-TL-PDMA, was finally obtained. The DP of PCL was calculated to be 135 by
12 ^1H NMR analysis *via* comparison of methyl groups (b, 2.8 ppm) in PDMA and methylene groups
13 next to ester the bonds (a, 4.1 ppm) (**Figure 1B, E**) and the block copolymer was denoted as
14 $\text{PCL}_{135}\text{-TL-PDMA}_{72}$. GPC traces of PDMA-TL-PCL showed a narrow molecular weight
15 distribution with M_w/M_n of 1.2. Next, the bock copolymer, PCL-PGEMA, was also synthesized
16 by using $\text{PCL}_{92}\text{-RAFT}$ to perform RAFT polymerization of GEMA in DMSO, and the actual DP
17 of PGEMA segment was calculated to be 38 (**Figures 1D and S4**), the obtained copolymer was
18 abbreviated as $\text{PCL}_{92}\text{-PGEMA}_{38}$. As a control, we also synthesized the block copolymer, $\text{PCL}_{137}\text{-}$
19 PDMA_{70} , with the ROS-nonresponsive linkage (**Figures 1C and S4**).

20
21
22
23
24
25
26
27
28
29
30
31
32
33
34
35
36
37
38
39
40
41
42
43
44
45
46
47
48
49
50
51
52
53
54
55
56
57
58
59
60

Subsequently, the obtained amphiphilic block polymers, PCL-TL-PDMA and PCL-PGEMA, were utilized to self-assemble into nanoparticles for encapsulation of PTX and Ce6 *via* the nanoprecipitation method. The different mixtures of PCL-TL-PDMA and PCL-PGEMA with the varying weight ratios of them were optimized for preparation of the nanoparticles and encapsulation of PTX and Ce6. The optimized PCL-TL-PDMA to PCL-PGEMA weight ratio of 5:2 was used to obtain the nanoparticles with the diameter of 90 ± 5 and size distribution of 0.15

1
2
3 **(Figure 1F)**. The loading capacities of Ce6 and PTX in the nanoparticles were determined to be
4
5 $6.8 \pm 0.31\%$ and 3.3 ± 0.01 , respectively. The nanoparticles were denoted as PCL-TL-NP_{PTX/Ce6}.
6
7 The TEM images showed an average diameter size of 70 ± 8 nm with a spherical structure
8
9 **(Figure 1G)**. Meanwhile, the PTX and Ce6-loaded nonresponsive nanoparticles from the
10
11 polymer mixture of PCL-PDMA and PCL-PGEMA with the weight ratio of 5:2 were also
12
13 formed with the PTX and Ce6 loading capacities of $6.6 \pm 0.26\%$ and $3.2 \pm 0.89\%$, respectively,
14
15 which was denoted as PCL-NP_{PTX/Ce6} and used as the control.
16
17

18
19 To evaluate the ROS generation of PCL-TL-NP_{PTX/Ce6} upon light irradiation, DPA was used
20
21 as the probe to determine the amount of produced ROS. As shown in **Figure 2A**, the intensity of
22
23 DPA fluorescence was stable without light irradiation of the nanoparticles. In sharp contrast, the
24
25 DPA fluorescence at 400 nm decreased quickly upon red light irradiation indicating the
26
27 production of singlet oxygen upon light irradiation.
28
29
30
31
32
33
34
35
36
37
38
39
40
41
42
43
44
45
46
47
48
49
50
51
52
53
54
55
56
57
58
59
60

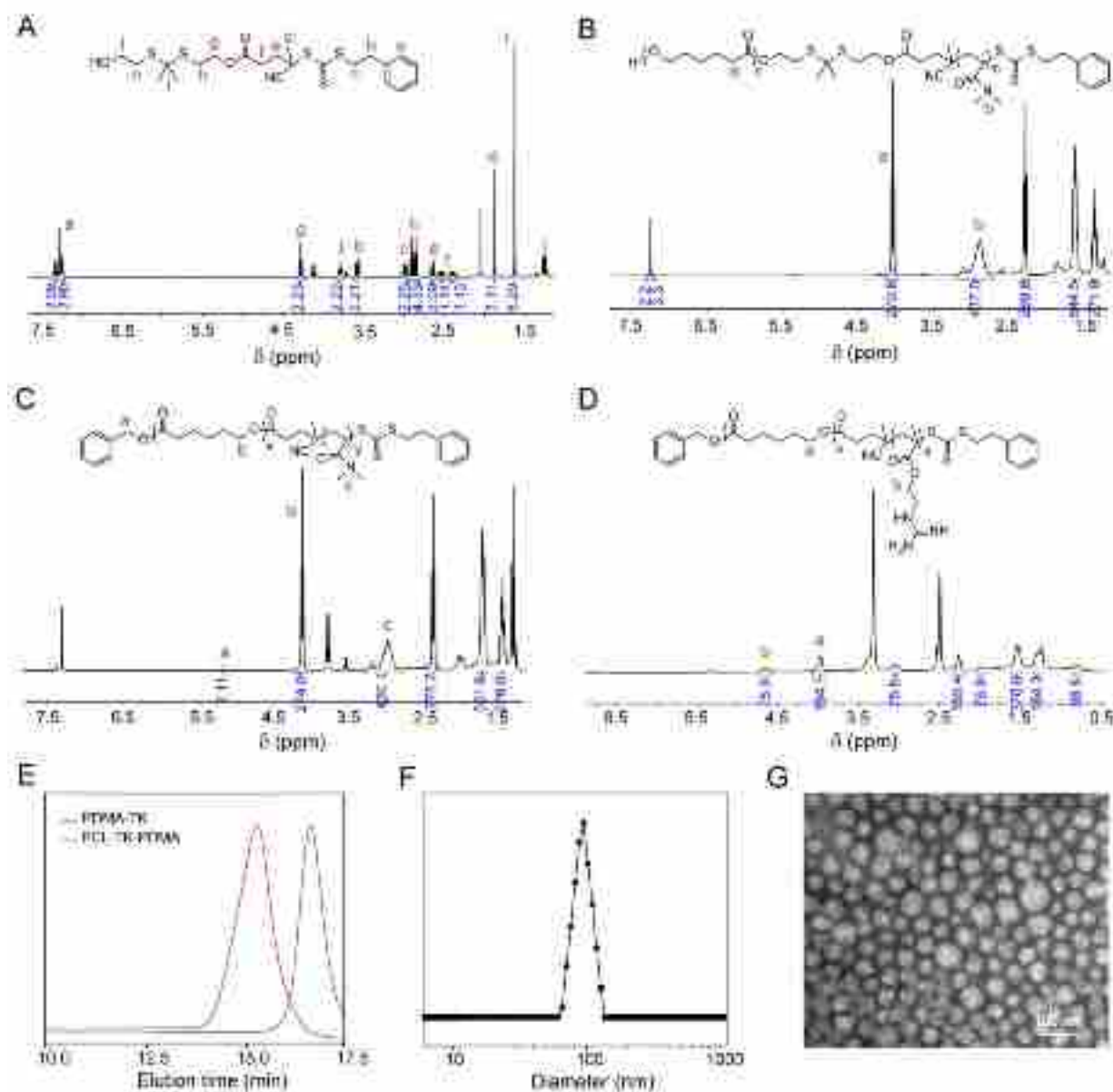
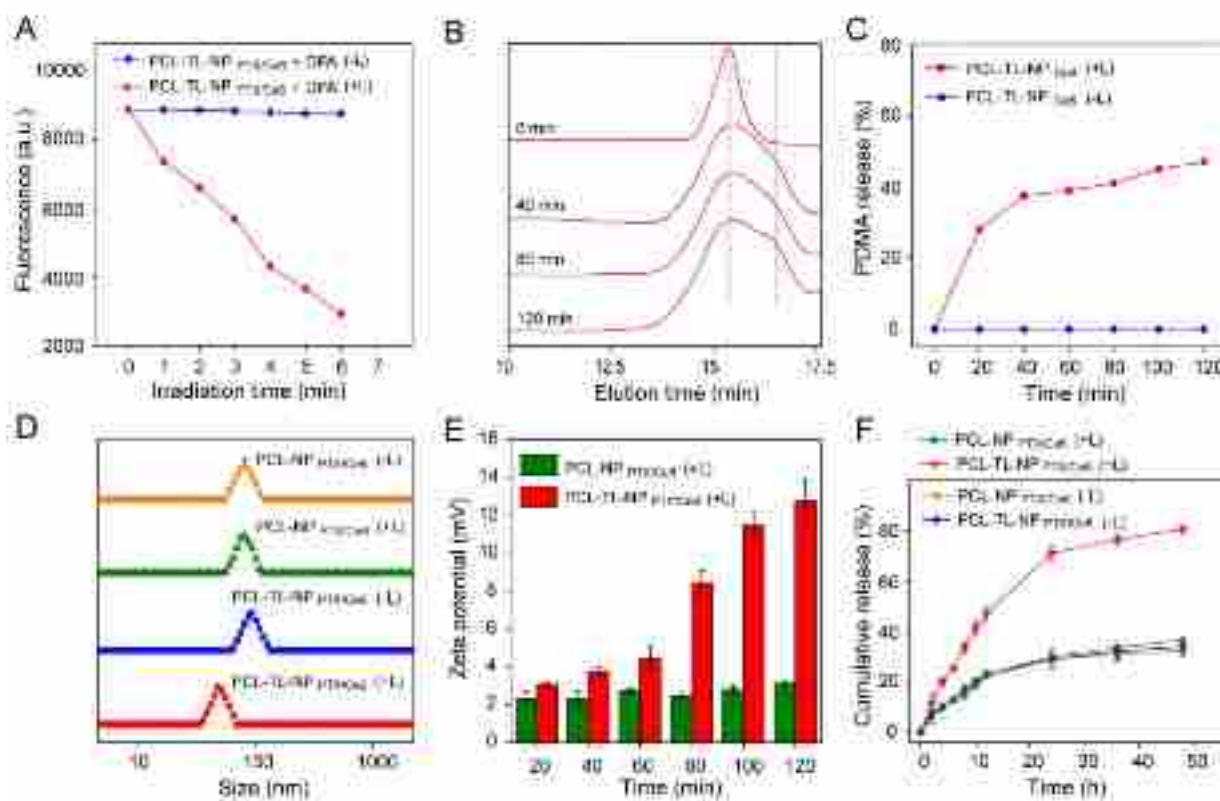


Figure 1. ^1H NMR spectra recorded for (A) macroRAFT-TL in CDCl_3 , (B) $\text{PCL}_{135}\text{-TL-PDMA}_{72}$ in CDCl_3 , (C) $\text{PCL}_{137}\text{-PDMA}_{70}$ in CDCl_3 , and (D) $\text{PCL}_{92}\text{-PGEMA}_{38}$ in $\text{DMSO-}d_6$. (E) GPC traces obtained for $\text{PDMA}_{72}\text{-TL}$ ($M_{n, \text{GPC}} = 7100$, $M_w/M_n = 1.13$) and $\text{PCL}_{135}\text{-TL-PDMA}_{72}$ ($M_n = 19200$, $M_w/M_n = 1.20$). (F) Nanoparticle size distribution of $\text{PCL-TL-NP}_{\text{PTX/Ce6}}$ by DLS analysis, and (G) TEM image of $\text{PCL-TL-NP}_{\text{PTX/Ce6}}$ after staining with uranyl acetate.

1
2
3 In addition, singlet oxygen produced by photosensitizer under light irradiation can efficiently
4 cleave TL moieties.^{40,47} To confirm that the cleavage of PCL-TL-PDMA can be achieved by the
5 produced singlet oxygen, we encapsulated Ce6 into PCL-TL-PDMA micellar nanoparticles with
6 the loading capacity of $3.6 \pm 0.11\%$ and the light irradiation was performed at the density of 80
7 mW/cm². The nanoparticle solutions after light irradiation were taken out and freeze-dried for
8 GPC measurement. As shown in **Figure 2B**, PCL-TL-PDMA exhibited elution volume peak at
9 15.2 min. Under 660 nm light irradiation, the peak at 16.5 min corresponding to PDMA appeared
10 and increased as an irradiation time feature. As shown in **Figure 2C**, the cleavage of PCL-TL-
11 PDMA is relatively rapid in the first 20 min with the ratio of 29% and increased gradually from
12 29% to more than 40% under continuous irradiation. In contrast, there was no degradation
13 observed in the absence of light irradiation. The results confirmed that the PDMA deshielding of
14 PCL-TL-PDMA-NP_{Ce6} was effectively accomplished under light irradiation due to the
15 photoinduced cleavage of TL linkages.
16
17
18
19
20
21
22
23
24
25
26
27
28
29
30
31
32

33 We further investigated the property changes of PCL-NP_{PTX/Ce6} and PCL-TL-NP_{PTX/Ce6}
34 including size, morphology, zeta potential, and stability with or without 660 nm red light
35 irradiation. As shown in **Figures 2D, S5 and S6**, size and size distribution measurements by
36 DLS as well as TEM observation for PCL-TL-NP_{PTX/Ce6} and PCL-NP_{PTX/Ce6} with or without light
37 irradiation were performed. DLS result showed an average size of PCL-TL-NP_{PTX/Ce6} decreased
38 from 90 ± 5 nm to 73 ± 3 nm with light irradiation for 120 min while the variation of PCL-
39 NP_{PTX/Ce6} size cannot be observed even after 120 min irradiation. The size decrease of PCL-TL-
40 NP_{PTX/Ce6} under light irradiation is presumably attributed to the partial cleavage of PDMA shells
41 after irradiation. Additionally, the influence of H₂O₂ on PCL-TL-NP_{PTX/Ce6} structure was also
42 shown in **Figure S5**, the average diameter of nanoparticle treated with 100 μ M H₂O₂ exhibited
43
44
45
46
47
48
49
50
51
52
53
54
55
56
57
58
59
60

no obvious change within 24 h, which should be attributed to very slow cleavage of PDMA under the low H_2O_2 concentration. TEM images for both nanoparticles before and after light irradiation showed no obvious change **Figure S6**. Presumably, TEM results were observed after the cleavage of PDMA from the nanoparticles, which did not affect their morphologies because the left PDMA and PGEMA shells can stabilize the nanoparticles well without obvious aggregation. These results suggested that the ROS produced within the core of the nanoparticle can effectively cleave the thioketal linker of PCL-TL-NP. Moreover, when PCL-NP_{PTX/Ce6} or PCL-TL-NP_{PTX/Ce6} was subjected to light irradiation for various time, the zeta potentials of PCL-NP_{PTX/Ce6} with or without light irradiation maintained constant (**Figures 2E and S7**). By contrast, the zeta potentials of PCL-TL-NP_{PTX/Ce6} increased from 1.8 mV to 13 mV, which can also be attributed to the release of the PDMA from the nanocarriers and exposure of positively charged PGEMA shells (**Figure 2E**).



1
2
3 **Figure 2.** (A) Singlet oxygen generation test of PCL-TL-NP_{PTX/Ce6} in the presence of DPA with
4 or without light irradiation of 660 nm at 80 mW/cm² for various times. (B) GPC traces of PCL-
5 TL-NP_{Ce6} with light irradiation for 40, 80, and 120 min. (C) Time-dependent PDMA release
6 from PCL-TL-NP_{Ce6} with or without light irradiation. (D) The particle size distribution with or
7 without light irradiation. (E) Zeta potential of PCL-NP_{PTX/Ce6} or PCL-TL-NP_{PTX/Ce6} after light
8 irradiation for different time. Mean \pm SD, n = 3. (F) Cumulative PTX release profiles of PCL-
9 TL-NP_{PTX/Ce6} and PCL-NP_{PTX/Ce6} with or without 660 nm light irradiation. Mean \pm SD, n = 3.

10
11
12
13
14
15
16
17
18
19 Additionally, PTX release profiles from the PCL-NP_{PTX/Ce6} and PCL-TL-NP_{PTX/Ce6}
20 nanocarriers with or without light irradiation were further evaluated. As shown in **Figure 2F**,
21 only ~ 23% of PTX released from PCL-NP_{PTX/Ce6} and PCL-NP_{PTX/Ce6} groups at 24 h regardless of
22 irradiation. In contrast, light-boosted PTX release from PCL-TL-NP_{PTX/Ce6} (+L) can be observed
23 with nearly 70% release at 24 h, which reflected faster release compared to PCL-TL-NP_{PTX/Ce6}
24 without light irradiation. The fast drug release under light irradiation is presumably attributed to
25 disturbance of singlet oxygen production and PDMA cleavage. Collectively, under 660 nm light
26 irradiation, PCL-TL-NP_{PTX/Ce6} nanoparticles showed effective ROS production which further
27 triggered partial PDMA release and accelerated drug release.

28
29
30
31
32
33
34
35
36
37
38
39
40 **Cellular uptake and intracellular ROS generation.** To evaluate the stability of PCL-TL-
41 NP_{PTX/Ce6} in cell culture medium, DLS analysis was carried out to monitor the size of the
42 nanoparticles after incubation in PBS solution containing 10% FBS. The average size of the
43 nanoparticles after incubation in PBS solution containing 10% FBS. The average size of the
44 nanoparticles remained unchanged up to 72 h of incubation at 37 °C (**Figure S8**), which
45 suggested that the long PDMA chains were able to stabilize PCL-TL-NP_{PTX/Ce6} avoiding
46 significant protein adsorption. Notably, deshielding PDMA shells from PCL-TL-NP_{PTX/Ce6} was
47 expected to enhance the cellular internalization.

1
2
3 Flow cytometry analysis was adapted to evaluate the internalization of PCL-TL-NP_{PTX/Ce6} in
4 HeLa cell line. The HeLa cells incubated with PCL-TL-NP_{PTX/Ce6} under light irradiation (+L) the
5 fluorescence intensities were much stronger than those without light irradiation at 4 h (**Figure**
6 **3A**). The cellular uptake efficiency was increased 2.1 folds with light irradiation. By comparison,
7 the cells treated with PCL-NP_{PTX/Ce6} (+L) did not showed an obvious increase in the fluorescence
8 intensity. Therefore, the enhanced intracellular fluorescence of PCL-TL-NP_{PTX/Ce6} (+L) should
9 be due to the fact that partial PDMA shells were efficiently deshielded from PCL-TL-NP_{PTX/Ce6}
10 under light irradiation for exposure of PGEMA as the cell-penetrating moieties.⁴¹ In addition,
11 CLSM observation was further used to investigate the intracellular distribution upon light
12 irradiation. As observed in **Figure S9**, the cellular uptake of PCL-NP_{PTX/Ce6} was not influenced
13 by light irradiation. Much higher intracellular green fluorescence for PCL-TL-NP_{PTX/Ce6} with
14 light irradiation for 40 min was obviously noted compared to cells treated by PCL-TL-NP_{PTX/Ce6}
15 without light irradiation (**Figure 3B, C**), which was in lines with the flow cytometry analysis
16 results. Next, we visualized intracellular ROS generation in HeLa cells after incubation with
17 PCL-NP_{PTX/Ce6} and PCL-TL-NP_{PTX/Ce6} by using DCFH-DA as the probe that can be oxidized
18 rapidly to DCFH by intracellular ROS to emit green fluorescence which can be used to quantify
19 ROS.⁴⁸ As demonstrated in **Figure 3D**, weak fluorescence was noted when the cells were treated
20 with PCL-NP_{PTX/Ce6} or PCL-TL-NP_{PTX/Ce6} without light irradiation. However, the DCF
21 fluorescence signals in cells treated with free Ce6, PCL-NP_{PTX/Ce6}, and PCL-TL-NP_{PTX/Ce6}
22 nanocarriers at 4 h after irradiation were significantly enhanced, confirming significantly
23 increased production of ROS inside cells under light irradiation due the presence of Ce6.
24 Moreover, when the cells were cultured with PCL-TL-NP_{PTX/Ce6} under light irradiation, HeLa
25 cells showed more intense green fluorescence. We also determined the mean fluorescence
26
27
28
29
30
31
32
33
34
35
36
37
38
39
40
41
42
43
44
45
46
47
48
49
50
51
52
53
54
55
56
57
58
59
60

intensity of ROS levels quantitatively by using flow cytometry (**Figure S10**). The ROS levels in PCL-TL-NP_{PTX/Ce6} treated cells displayed a considerably greater induction effect on the ROS generation after irradiation by 660 nm light as compared with other groups, which was likely due to the fact that the cleavage of PDMA shells on PCL-TL-NP_{PTX/Ce6} (+L) enhanced the cellular uptake efficiency and improved intracellular ROS generation.

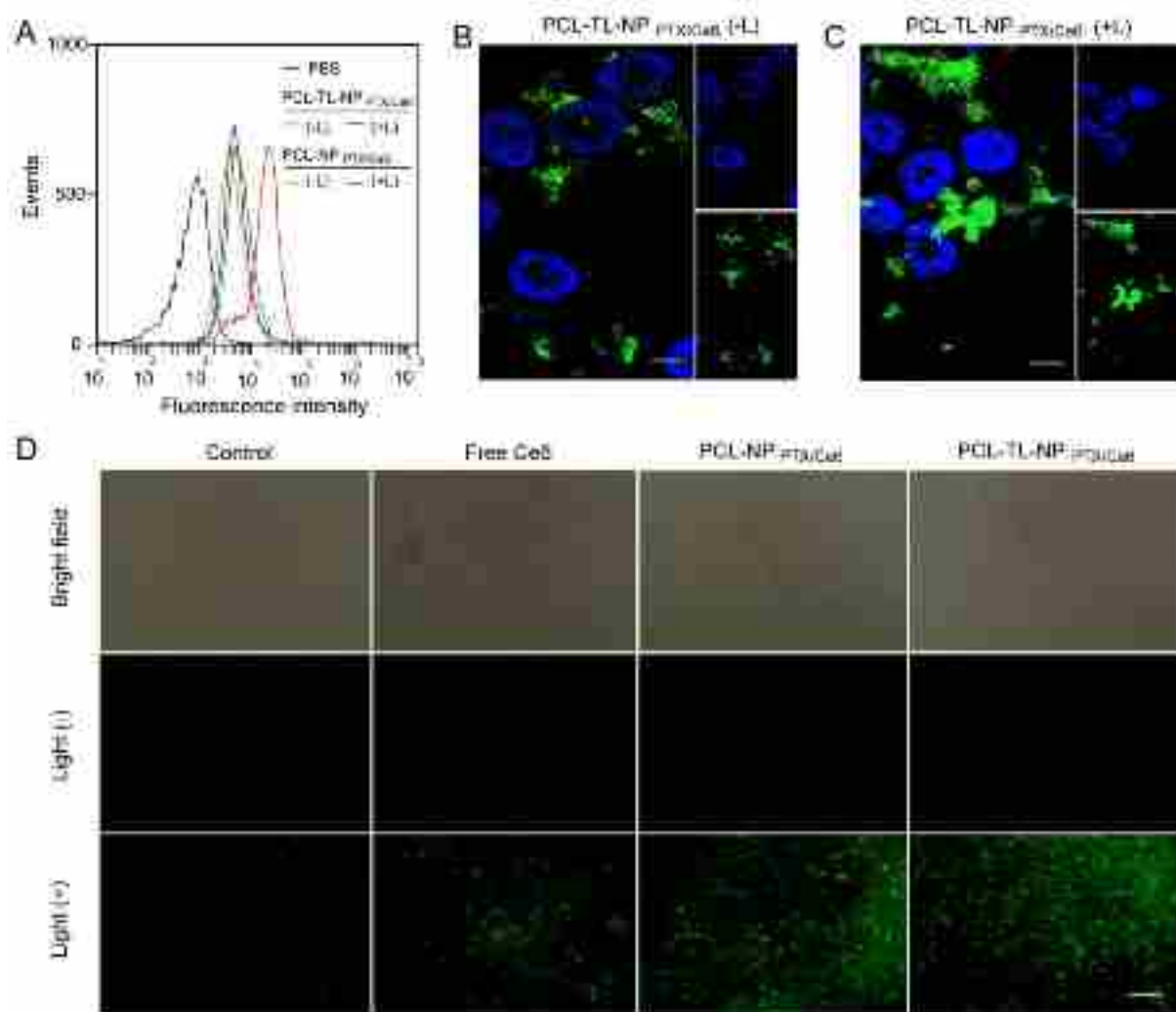


Figure 3. (A) Cellular uptake of HeLa cells by flow cytometry analysis after treatment by PBS, PCL-NP_{PTX/Ce6} and PCL-TL-NP_{PTX/Ce6} at the PTX concentration of 4.0 $\mu\text{g}/\text{mL}$ and Ce6 of 1.94 $\mu\text{g}/\text{mL}$ with or without light irradiation followed by incubation for 4 h. (B, C) Cellular uptake observation by CLSM of HeLa cells after treatment by PCL-TL-NP_{PTX/Ce6} (-L) and (+L)

1
2
3 followed by further incubation for 4 h. Cell nuclei were counterstained with DAPI (blue). The
4 scale bar is 20 μm . (D) Intracellular ROS level in HeLa cells after treatment by PBS, free Ce6,
5 PCL-NP_{Ce6/PT}, and PCL-TL-NP_{PTX/Ce6} with or without light irradiation by using DCFH-DA as the
6 probe. Scale bar is 20 μm .
7
8
9

10
11
12
13
14 ***In vitro* cytotoxicity.** In order to evaluate the cytotoxicity of the nanoparticles against HeLa cell
15 line, MTT assay, live/dead assay, and flow cytometry analysis were performed respectively.
16 Briefly, HeLa cells were incubated with varying concentrations of free PTX/Ce6, PCL-TL-
17 NP_{Ce6}, PCL-TL-NP_{PTX}, PCL-NP_{PTX/Ce6}, or PCL-TL-NP_{PTX/Ce6} with or without light irradiation.
18 From the cell viability in **Figure S11**, it was observed that the combined treatment by free
19 PTX/Ce6 showed slightly higher cytotoxicity under light irradiation with IC50 of 2.6 $\mu\text{g/mL}$
20 PTX at the corresponding Ce6 concentration of 1.26 $\mu\text{g/mL}$ as compared with that of 3.2 $\mu\text{g/mL}$
21 PTX without light. Moreover, as shown in **Figure 4A**, although it was observed that PCL-
22 NP_{PTX/Ce6} demonstrated a moderate cell killing efficacy, the red light irradiation did not show
23 much difference with the comparable IC50 values of 5.2 $\mu\text{g/mL}$ (+L) and 5.9 $\mu\text{g/mL}$ (-L) PTX,
24 which could be due to relatively low cellular internalization and light-nonresponsive properties
25 of the nanoparticles. In a sharp contrast, the irradiation showed great potential to improve the
26 cell cytotoxicity of PCL-TL-NP_{PTX/Ce6} with IC50 of 2.3 $\mu\text{g/mL}$ PTX at the corresponding Ce6
27 concentration of 1.12 $\mu\text{g/mL}$, which was 2.56 folds lower than the treatment without light and
28 significantly lower than any other cytotoxicity efficacy among the evaluated formulations
29 (**Figure 4B**). The highest cytotoxicity of PCL-TL-NP_{PTX/Ce6} under light irradiation can be
30 presumably elucidated by the fact that the encapsulated Ce6 can be excited to generate ROS for
31 PDT and also cleavage of the thioketal linkers for cellular uptake and PTX release.
32
33
34
35
36
37
38
39
40
41
42
43
44
45
46
47
48
49
50
51
52
53
54
55
56
57
58
59
60

1
2
3 Nevertheless, in **Figure S12**, the treatment with TL-linked nanoparticles either loading only
4 Ce6 or PTX (PCL-TL-NP_{Ce6} or PCL-TL-NP_{PTX}) in the presence of light irradiation showed
5 relatively low cytotoxicity with IC₅₀ of 3.1 μg/mL Ce6 and 6.4 μg/mL PTX, respectively, which
6 suggested the significance of combined therapy. Subsequently, the synergism behavior of PTX
7 and Ce6 in PCL-TL-NP_{PTX/Ce6} was evaluated by calculation of combination index (CI) of their
8 IC₅₀ values according to Chou-Talalay's isobolographic method based on the Equation 1.^{46,49}
9
10 From **Figure 4C**, it was observed that the CI value was significantly improved with the
11 increasing of both Ce6 and PTX concentrations during treatment. Specifically, the calculated CI
12 in the range between 0.93 and 0.15 for all fraction affected suggested a strong degree of
13 synergism between PTX and Ce6. Therefore, the observed high cell killing capability for PCL-
14 TL-NP_{PTX/Ce6} under light irradiation can also be elucidated by the strong synergistic effect
15 between the integrated PTX and Ce6 to achieve pronounced cytotoxicity against HeLa cells.
16
17
18
19
20
21
22
23
24
25
26
27
28
29

30
31 Next, after treatment of HeLa cells with PCL-NP_{PTX/Ce6}, and PCL-TL-NP_{PTX/Ce6} with or
32 without light irradiation at the PTX equivalent concentration of 4.0 μg/mL and Ce6 of 1.94
33 μg/mL, live/dead assay was further performed by FDA and PI co-staining cells to evaluate live
34 (green) and dead cells (red), respectively. From **Figure 4D**, it was observed that at 24 h after
35 light irradiation, PCL-NP_{PTX/Ce6} exhibited slightly increased ratio of dead cells compared to that
36 without light. By contrast, PCL-TL-NP_{PTX/Ce6} showed remarkably increased red area than that
37 without light irradiation, which was in good agreement with the MTT outcomes and further
38 confirmed the high cytotoxicity results of PCL-TL-NP_{PTX/Ce6} (+L).
39
40
41
42
43
44
45
46
47
48
49
50
51
52
53
54
55
56
57
58
59
60

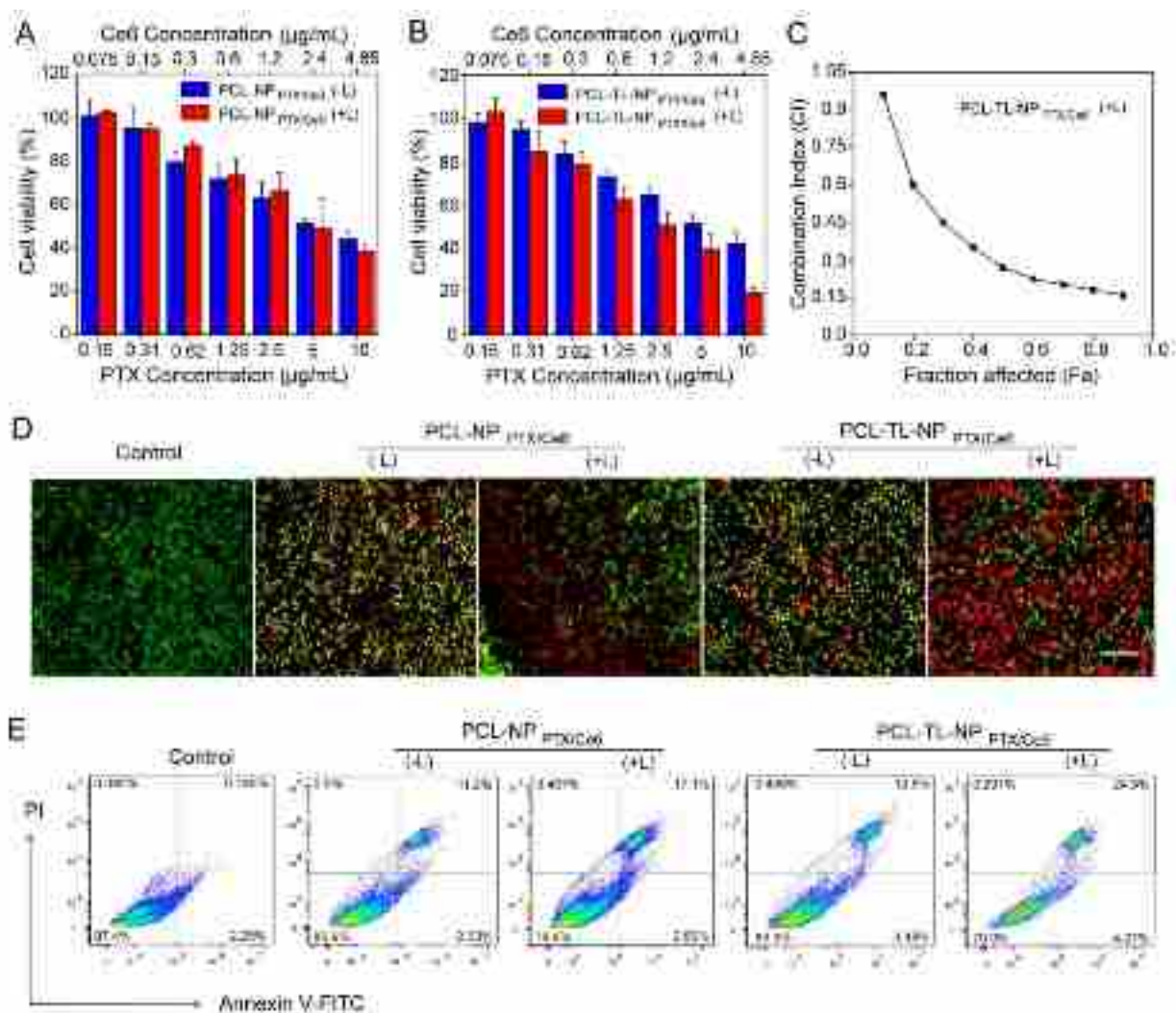


Figure 4. (A, B) Cytotoxicity in HeLa cells after treatment by PCL-NP_{PTX/Ce6} or PCL-TL-NP_{PTX/Ce6} with or without light irradiation at different concentrations of PTX and Ce6. Mean \pm SD, n = 4. (C) The combined index (CI) synergy trends with various ratiometric mixtures of PTX and Ce6 for PCL-TL-NP_{PTX/Ce6} (+L). (D) Live and dead staining images of HeLa cells at 24 h after incubation with PCL-NP_{PTX/Ce6} or PCL-TL-NP_{PTX/Ce6} with or without light irradiation at the PTX equivalent concentration of 4.0 μ g/mL and Ce6 of 1.94 μ g/mL. Scale bar represents 20 μ m. (E) Cell apoptosis analysis of HeLa cells by flow cytometer after incubation with PCL-NP_{PTX/Ce6} or PCL-TL-NP_{PTX/Ce6} with or without light irradiation at the equivalent concentration of 4.0 μ g/mL PTX and 1.94 μ g/mL Ce6.

1
2
3
4
5
6
7
8
9
10
11
12
13
14
15
16
17
18
19
20
21
22
23
24
25
26
27
28
29
30
31
32
33
34
35
36
37
38
39
40
41
42
43
44
45
46
47
48
49
50
51
52
53
54
55
56
57
58
59
60

Moreover, we further evaluated the cell apoptosis by staining HeLa cells with Annexin V/propidium iodide (PI) assay and flow cytometer analysis after treating with PCL-NP_{PTX/Ce6}, or PCL-TL-NP_{PTX/Ce6} with or without light irradiation at the PTX equivalent concentration of 4.0 $\mu\text{g/mL}$ and Ce6 of 1.94 $\mu\text{g/mL}$ (**Figure 4E**). It was observed that PCL-NP_{PTX/Ce6} and PCL-TL-NP_{PTX/Ce6} without light irradiation induced comparable apoptosis of 11.2% and 12.8%, respectively, against HeLa cells. However, when the HeLa cells were treated with PCL-NP_{PTX/Ce6} (+L), the apoptotic cells levels were modestly raised to 17%. Notably, the cells treated with PCL-TL-NP_{PTX/Ce6} (+L) induced 24.5% cell apoptosis, which was determined to be the highest cellular apoptotic rate. In overall, the cytotoxicity evaluation validated that the synergistic effect of PCL-TL-NP_{PTX/Ce6} nanocarriers can induce significantly enhanced cancer cell killing efficacy due to more effective cell uptake and synergistic effect of PDT and chemotherapy inside cells.

***In vivo* biodistribution and ROS production.** Female BALB/c mice bearing H22 model ($\sim 60 \text{ mm}^3$) were used to evaluate biodistribution and intratumor ROS level after intravenous injection of PCL-NP_{PTX/Ce6} or PCL-TL-NP_{PTX/Ce6} upon exposure to light irradiation. Briefly, the nanoparticles were intravenously injected *via* the tail vein. Given that the nanoparticles can emit fluorescence due to the loaded Ce6 photosensitizer, the biodistribution was monitored by using IVIS imaging system at predetermined time intervals of 1, 6, 12, 24, or 48 h, respectively, post injection. As observed in **Figure 5A**, the comparable fluorescence intensity of Ce6 at the tumor site for either PCL-TL-NP_{PTX/Ce6} or PCL-TL-NP_{PTX/Ce6} treated groups were time-dependent and gradually increased to the highest intensity at 12 h post injection. In addition, the detectable amount of fluorescence was still available even at 48 h post-injection, which showed that the nanoparticles could accumulate efficiently at the tumor site *via* EPR effect with a prolonged

1
2
3 bioavailability. Subsequently, the mice were sacrificed at 48 h after the post injection, followed
4
5 by collecting the major organs and tumor tissues for fluorescence imaging (**Figure S13A, B**).
6
7 Although quantifiable amount of Ce6 fluorescence can still be detected at 48 h in major organs
8
9 such as kidney and liver, the significantly enhanced accumulation of PCL-TL-NP_{PTX/Ce6} in the
10
11 tumor was observed which is ~1.5-fold more than the fluorescence intensity in liver and ~ 2-fold
12
13 in kidney.
14
15

16
17 Furthermore, to evaluate the blood circulation of free PTX, PCL-NP_{PTX/Ce6}, and PCL-TL-
18
19 NP_{PTX/Ce6}, H22 tumor-bearing BALB/c mice were administered intravenously *via* the tail vein
20
21 with free PTX, PCL-NP_{PTX/Ce6}, or PCL-TL-NP_{PTX/Ce6}, at a PTX-equivalent dose of 10 mg/kg.
22
23 The blood samples were collected at specified post-injection time intervals, and PTX levels were
24
25 calculated as a function of time using HPLC. From **Figure 5B**, it was clearly observed that PCL-
26
27 NP_{PTX/Ce6} and PCL-TL-NP_{PTX/Ce6} exhibited similar blood circulation curves with considerably
28
29 long circulation time compared to free PTX. Additionally, the accumulation of both PCL-
30
31 NP_{PTX/Ce6} and PCL-TL-NP_{PTX/Ce6} in the major organs such as heart, liver, spleen, lung, and
32
33 kidney as well as in the tumor at 48 h post injection also showed similar bioavailability for PTX
34
35 (**Figure 5C**), likely due to the similar physicochemical properties of both nanoparticles. Overall,
36
37 PCL-TL-NP_{PTX/Ce6} with the coverage of long hydrophilic PDMA shells could prolong circulation
38
39 in the blood stream and accumulate in tumor tissues, which can potentiate therapeutic effects
40
41 through synergistic combination of PDT and chemotherapy.
42
43
44
45
46
47
48
49
50
51
52
53
54
55
56
57
58
59
60

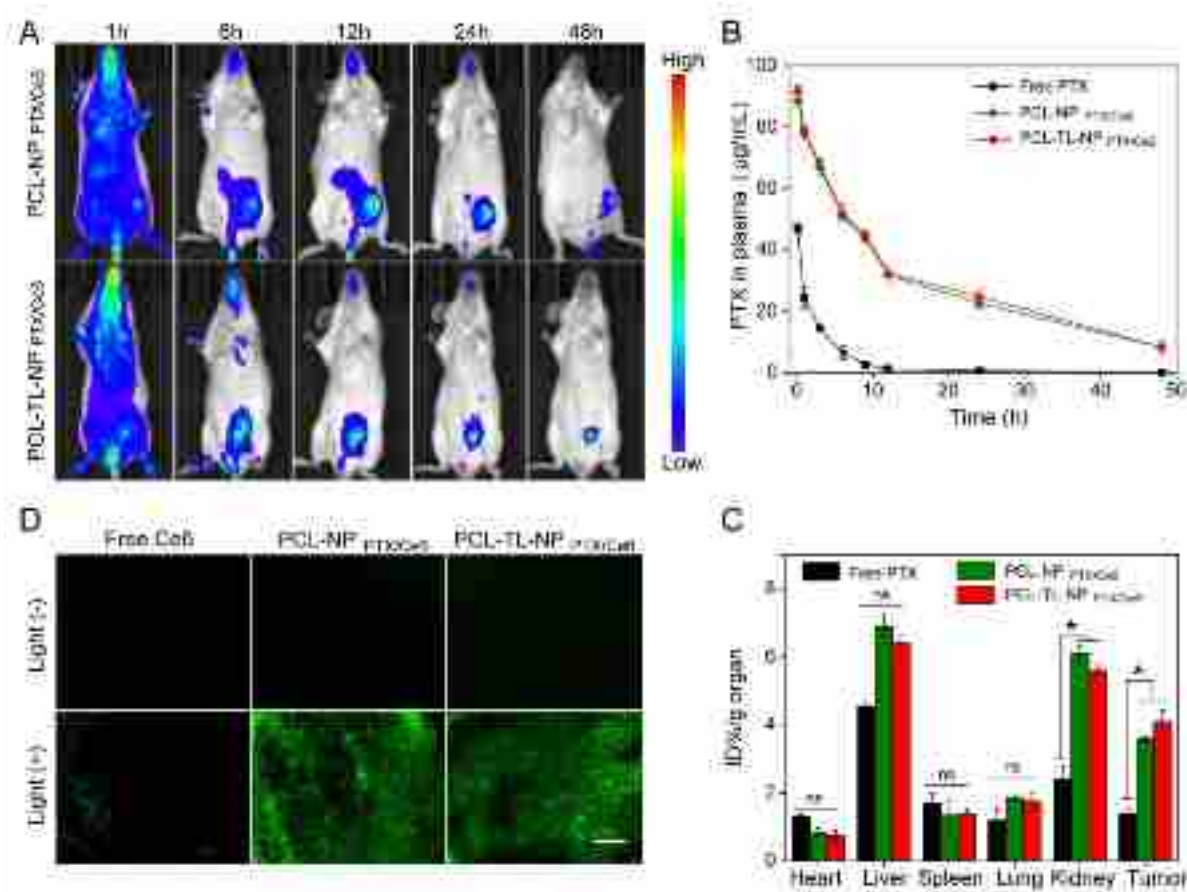


Figure 5. (A) *In vivo* biodistribution analysis by IVIS imaging of H22 tumor-bearing mice after the intravenous injection of PCL-NP_{PTX/Ce6} and PCL-TL-NP_{PTX/Ce6} at various predetermined post injection time periods. (B) Blood circulation evaluation by plasma PTX concentration versus time courses after free PTX, PCL-TL-NP_{PTX/Ce6}, and PCL-TL-NP_{PTX/Ce6} injection intravenously. Mean \pm SD, $n = 3$. (C) Quantification of the PTX concentrations in major organs at 48 h post-injection. Mean \pm SD, $n = 3$. * $p < 0.05$. Ns means no significant. (D) Intratumor ROS levels after intravenous injection of various formulations by fluorescence images of H22 tumor sections at 24 h. The scale bar is 20 μ m.

To investigate the ROS production in the tumor tissues, injection of BALB/c mice bearing H22 tumor model with free Ce6, PCL-NP_{PTX/Ce6}, or PCL-TL-NP_{PTX/Ce6}, followed by intratumoral injection of DCFH-DA ROS probe and light irradiation for 40 min. Subsequently, mice were euthanized and tumor sections were collected for ROS generation evaluation based on the

1
2
3 intensity of green fluorescence emitted by the oxidized DCFH-DA product. From **Figure 5D**,
4 relatively low fluorescence intensity was observed when mice were treated with PCL-NP_{PTX/Ce6},
5 PCL-TL-NP_{PTX/Ce6} or Ce6 without light irradiation, which can be attributed to the intrinsic and
6 heterogeneous distributed ROS (e.g., H₂O₂) level in tumor tissue.^{50,51} Moreover, the treatment
7 with free Ce6 and PCL-NP_{PTX/Ce6} under light irradiation showed low green fluorescence intensity
8 which can be possibly explained by inefficient accumulation of free Ce6 and impaired release of
9 loaded materials for PCL-NP_{PTX/Ce6} at the tumor site, respectively. In sharp contrast, PCL-
10 NP_{PTX/Ce6} (+L) and PCL-TL-NP_{PTX/Ce6} (+L) were exhibited strong fluorescence intensity as
11 compared with free Ce6 (+L), owing to their efficient tumor accumulation. Therefore, it was
12 demonstrated that PCL-TL-NP_{PTX/Ce6} can generate high amount of ROS which can trigger
13 PDMA release and accelerate PTX release at the tumor site when exposed to the 660 nm red
14 light.

15
16
17 ***In vivo* antitumor efficacy.** Encouraged by the observed enhanced cell killing efficacy of PCL-
18 TL-NP_{PTX/Ce6} (+L) from *in vitro* results and improved tumor accumulation, we then performed
19 the *in vivo* antitumor investigation of PCL-TL-NP_{PTX/Ce6} to evaluate the advantages of our
20 designed nanocarriers. Briefly, BALB/c mice bearing H22 tumor model (~ 60 mm³) were
21 blindfolded divided into 7 treatment groups which are PBS, free Ce6 (+L), free PTX, PCL-
22 NP_{PTX/Ce6} (-L), PCL-TL-NP_{PTX/Ce6} (-L), PCL-NP_{PTX/Ce6} (+L), or PCL-TL-NP_{PTX/Ce6} (+L) at PTX-
23 equivalent doses of 2.5 mg/kg and Ce6 of 1.21 mg/kg *via* i.v. injection. After 24 h post
24 administration, the tumor site was irradiated for 40 min by 660 nm red light at a power density of
25 80 mW/cm², and then the tumor growth was monitored. We chose 40 min irradiation due to our
26 preliminary experiment results as shown in **Figure 2C**. The cleavage of PDMA is more than
27 40% under continuous irradiation of 40 min, which can significantly enhance the cellular uptake
28
29
30
31
32
33
34
35
36
37
38
39
40
41
42
43
44
45
46
47
48
49
50
51
52
53
54
55
56
57
58
59
60

1
2
3 and subsequently boosts effective drug release. From **Figure 6A, B**, it was observed that the
4 treatment with PCL-TL-NP_{PTX/Ce6} and PCL-NP_{PTX/Ce6} without light irradiation showed
5 comparable tumor growth inhibition effect with 13.2-fold and 11.6-fold tumor size increase,
6 respectively. In comparison to the PCL-NP_{PTX/Ce6} (L+)-treated group which showed mild tumor
7 growth inhibition with 11.8-fold tumor size increase at day 21, PCL-TL-NP_{PTX/Ce6} (+L) exhibited
8 the highest tumor growth inhibition rate with only 2.1-fold tumor size increase at day 21 post
9 treatment, which was also supported by *ex vivo* tumor weigh evaluation and tumor digital images
10 (**Figure 6B, D**). The remarkably improved anticancer efficacy of PCL-TL-NP_{PTX/Ce6} (+L) was
11 possibly due to the synergistic effect of photoinduced improved intracellular drug delivery and
12 combined photodynamic and chemo-therapy.
13
14
15
16
17
18
19
20
21
22
23
24
25

26 Although the mice body weight monitoring during treatment didn't show obvious change for
27 all formulations used, suggesting low side toxicity of these treatments (**Figure 6C**), the
28 histological analysis of the tumor sections stained by H&E showed the greatest level of tumor
29 tissue damage after treatment with PCL-TL-NP_{PTX/Ce6} (+L) (**Figure 6E**). Additionally, the
30 histologic images of major organs analyzed by H&E staining also did not show obvious
31 biological toxicity on the heart, liver, spleen, lung and kidney, for PCL-TL-NP_{PTX/Ce6} with or
32 without light irradiation treated groups, further confirming low side toxicity of PCL-TL-
33 NP_{PTX/Ce6} (**Figure S14**). Collectively, *in vivo* results showed that PCL-TL-NP_{PTX/Ce6} (+L) can
34 achieve superior anticancer efficacy without high side effects through synergistically combined
35 PDT with chemotherapy.
36
37
38
39
40
41
42
43
44
45
46
47
48
49
50
51
52
53
54
55
56
57
58
59
60

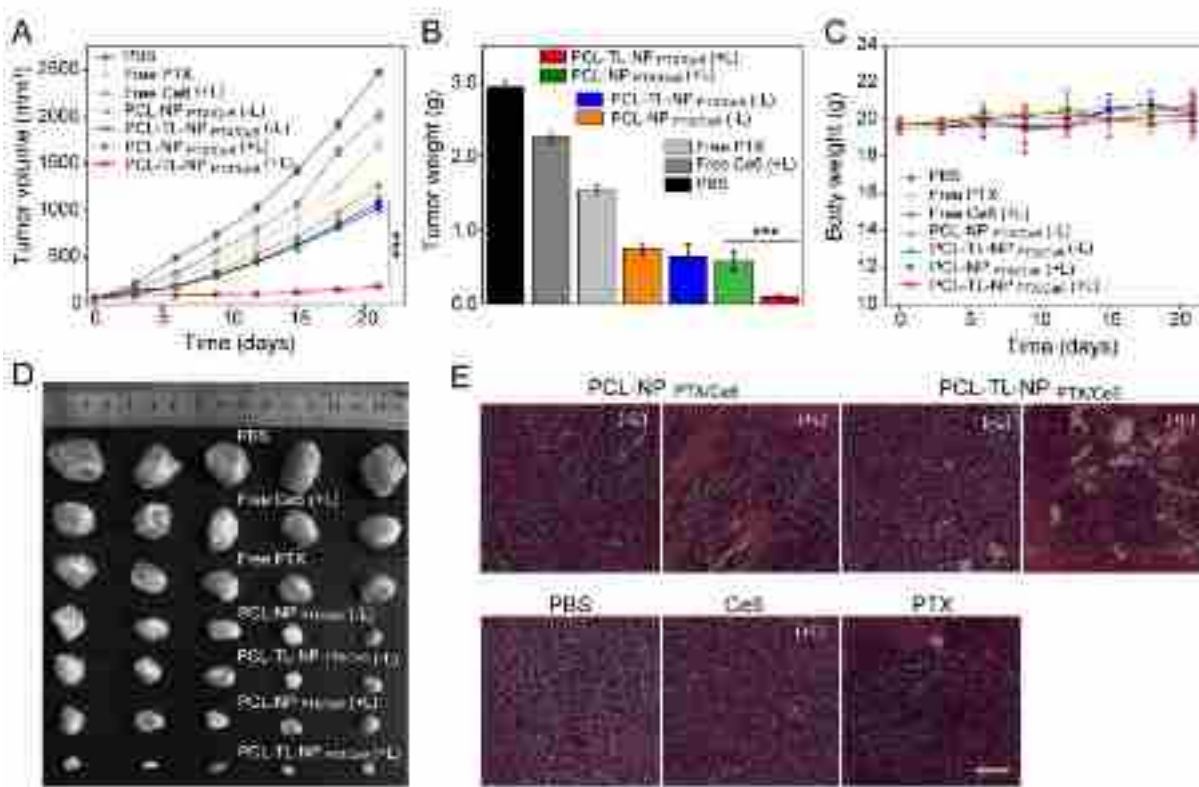


Figure 6. (A) H22 tumors growth curves of the mice treated with various formulations at a PTX equivalent dose of 2.5 mg/kg or a Ce6 dose of 1.21 mg/kg with 40 min light irradiation (660 nm, 80 mW/cm²) or without light (mean \pm SD, n = 5). (B) Tumor weights at the end of the treatments. (C) Body weight monitoring of the mice that received treatments with various formulations. (D) Photographs of the tumors at day 21 post treatment. (E) H&E staining analysis of the tumor tissues after various treatments. The scale bar is 20 μ m. ***p < 0.005.

CONCLUSIONS

In conclusion, we designed a unique type of ROS-responsive nanocarriers that co-encapsulated PTX and Ce6. Under light irradiation, PCL-TL-NP_{PTX/Ce6} nanocarriers were able to efficiently produce ROS from the encapsulated Ce6, which led to the cleavage of thioketal linkers. Subsequently, the PDMA shells were partially deshielded from PCL-TL-NP_{PTX/Ce6}, which resulted in exposure of cell-penetrating moieties of PGEMA and enhancement of the

cellular uptake. Moreover, PCL-TL-NP_{PTX/Ce6} showed significant synergistic effects on cell killing ability by PDT and chemotherapy under light irradiation. The *in vivo* results showed that PCL-TL-NP_{PTX/Ce6} (+L) efficiently inhibited H22 tumor growth. Therefore, all these results suggested that PCL-TL-NP_{PTX/Ce6} nanocarriers could be used as novel nanocarriers for the combined of PDT and chemotherapy through photoinduced enhancement of cellular internalization and drug release.

ASSOCIATED CONTENT

Supporting Information

Characterization instruments; synthetic routes for preparation of PCL-TL-PDMA, PCL-PDMA, PCL-PGEMA; ¹³C NMR and ESI-MS analysis of RAFT-TL; ¹H NMR of polymer PDMA-MacroRAFT-TL and GPC characterizations of PCL-PDMA, PCL-PGEMA; Stability of PCL-NP_{PTX/Ce6} and PCL-TL-NP_{PTX/Ce6}; CLSM images, intracellular ROS level; Cytotoxicity of PTX/Ce6 with (+L) without light (-L), PCL-TL-NP_{Ce6} (+L), and PCL-TL-NP_{PTX} (+L); Biodistribution of major organs images; H&E-stained images. This material is available free of charge via the Internet at <http://pubs.acs.org>.

AUTHOR INFORMATION

Corresponding Author

* Email: gez@ustc.edu.cn (Z. Ge)

Author Contributions

† These authors contributed equally to the work.

Notes

The authors declare no competing financial interest.

ACKNOWLEDGMENT

We gratefully acknowledge financial support from National Natural Science Foundation of China (NNSFC) Project (21674104, 21875234) and CAS-TWAS presidents Fellowship for Ph.D. Scholarship.

REFERENCES

- (1) Peer, D.; Karp, J. M.; Hong, S.; Farokhzad, O. C.; Margalit, R.; Langer, R. Nanocarriers as an Emerging Platform for Cancer Therapy. *Nat. Nanotechnol.* **2007**, *2*, 751-760.
- (2) Lobatto, M. E.; Fuster, V.; Fayad, Z. A.; Mulder, W. J. Perspectives and Oportunities for Nanomedicine in the Management of Atherosclerosis. *Nat. Rev. Drug Discovery* **2011**, *10*, 835-852.
- (3) Wang, L.; Hu, C.; Shao, L. The Antimicrobial Activity of Nanoparticles: Present Situation and Prospects for the Future. *Int. J. Nanomed.* **2017**, *12*, 1227-1249.
- (4) Sun, Q. H.; Zhou, Z. X.; Qiu, N. S.; Shen, Y. Q. Rational Design of Cancer Nanomedicine: Nanoproperty Integration and Synchronization. *Adv. Mater.* **2017**, *29*, 1606628. doi: 10.1002/adma.201606628.
- (5) Min, Y. Z.; Caster, J. M.; Eblan, M. J.; Wang, A. Z. Clinical Translation of Nanomedicine. *Chem. Rev.* **2015**, *115*, 11147-11190.
- (6) Cabral, H.; Kataoka, K. Progress of Drug-Loaded Polymeric Micelles into Clinical Studies. *J. Controlled Release* **2014**, *190*, 465-476.

- 1
2
3 (7) Cabral, H.; Miyata, K.; Osada, K.; Kataoka, K. Block Copolymer Micelles in Nanomedicine
4 Applications. *Chem. Rev.* **2018**, *118*, 6844-6892.
5
6
7 (8) Mok, H.; Park, J. W.; Park, T. G. Enhanced Intracellular Delivery of Quantum Dot and
8 Adenovirus Nanoparticles Triggered by Acidic pH via Surface Charge Reversal. *Bioconjugate*
9 *Chem.* **2008**, *19*, 797-801.
10
11
12 (9) Ke, W. D.; Yin, W.; Zha, Z. S.; Mukerabigwi, J. F.; Chen, W. J.; Wang, Y. H.; He, C. X.;
13 Ge, Z. S. A Robust Strategy for Preparation of Sequential Stimuli-Responsive Block Copolymer
14 Prodrugs via Thiolactone Chemistry to Overcome Multiple Anticancer Drug Delivery Barriers.
15 *Biomaterials* **2018**, *154*, 261-274.
16
17
18 (10) Chen, X. L.; Liu, L. S.; Jiang, C. Charge-Reversal Nanoparticles: Novel Targeted Drug
19 Delivery Carriers. *Acta Pharm. Sin. B* **2016**, *6*, 261-267.
20
21
22 (11) Yang, X. Z.; Du, X. J.; Liu, Y.; Zhu, Y. H.; Liu, Y. Z.; Li, Y. P.; Wang, J. Rational Design
23 of Polyion Complex Nanoparticles to Overcome Cisplatin Resistance in Cancer Therapy. *Adv.*
24 *Mater.* **2014**, *26*, 931-936.
25
26
27 (12) Huang, M. M.; Zhao, K. J.; Wang, L.; Lin, S. Q.; Li, J. J.; Chen, J. B.; Zhao, C. G.; Ge, Z.
28 S. Dual Stimuli-Responsive Polymer Prodrugs Quantitatively Loaded by Nanoparticles for
29 Enhanced Cellular Internalization and Triggered Drug Release. *ACS Appl. Mater. Interfaces*
30 **2016**, *8*, 11226-11236.
31
32
33 (13) Sun, C. Y.; Liu, Y.; Du, J. Z.; Cao, Z. T.; Xu, C. F.; Wang, J. Facile Generation of Tumor-
34 pH-Labile Linkage-Bridged Block Copolymers for Chemotherapeutic Delivery. *Angew. Chem.*
35 *Int. Ed.* **2016**, *55*, 1010-1014.
36
37
38 (14) Ke, W. D.; Zha, Z. S.; Mukerabigwi, J. F.; Chen, W. J.; Wang, Y. H.; He, C. X.; Ge, Z. S.
39 Matrix Metalloproteinase-Responsive Multifunctional Peptide-Linked Amphiphilic Block
40
41
42
43
44
45
46
47
48
49
50
51
52
53
54
55
56
57
58
59
60

1
2
3 Copolymers for Intelligent Systemic Anticancer Drug Delivery. *Bioconjugate Chem.* **2017**, *28*,
4 2190-2198.
5

6
7 (15) Kong, L.; Campbell, F.; Kros, A. DePEGylation Strategies to Increase Cancer
8 Nanomedicine Efficacy. *Nanoscale Horiz.* **2019**, *4*, 378-387.
9

10
11 (16) Jiang, W.; Wang, J. L.; Yang, J. B.; He, Z. W.; Hou, Z. H.; Luo, Y. L.; Wang, L.; Liu, J.;
12 Zhang, H. B.; Zhao, Y. Y.; Zhang, G. Q.; Huang, F.; Zhou, X. C.; Yan, L. F.; Yang, X. Z.;
13 Wang, Y. C.; Wang, J. Acidity-Triggered TAT-Presenting Nanocarriers Augment Tumor
14 Retention and Nuclear Translocation of Drugs. *Nano Res.* **2018**, *11*, 5716-5734.
15
16

17
18 (17) Jin, E. L.; Zhang, B.; Sun, X. R.; Zhou, Z. X.; Ma, X. P.; Sun, Q. H.; Tang, J. B.; Shen, Y.
19 Q.; Van Kirk, E.; Murdoch, W. J.; Radosz, M. Acid-Active Cell-Penetrating Peptides for in Vivo
20 Tumor-Targeted Drug Delivery. *J. Am. Chem. Soc.* **2013**, *135*, 933-940.
21
22

23
24 (18) Wang, S.; Yu, G. C.; Wang, Z. T.; Jacobson, O.; Tian, R.; Lin, L. S.; Zhang, F. W.; Wang,
25 J.; Chen, X. Y. Hierarchical Tumor Microenvironment-Responsive Nanomedicine for
26 Programmed Delivery of Chemotherapeutics. *Adv. Mater.* **2018**, *30*, 1803926. doi:
27 10.1002/adma.201803926.
28
29

30
31 (19) Zhu, L.; Wang, T.; Perche, F.; Taigind, A.; Torchilin, V. P. Enhanced Anticancer Activity
32 of Nanopreparation Containing an MMP2-Sensitive PEG-Drug Conjugate and Cell-Penetrating
33 Moiety. *Proc. Natl. Acad. Sci. U. S. A.* **2013**, *110*, 17047-17052.
34
35

36
37 (20) Cheng, H.; Zhu, J. Y.; Xu, X. D.; Qiu, W. X.; Lei, Q.; Han, K.; Cheng, Y. J.; Zhang, X. Z.
38 Activable Cell-Penetrating Peptide Conjugated Prodrug for Tumor Targeted Drug Delivery. *ACS*
39 *Appl. Mater. Interfaces* **2015**, *7*, 16061-16069.
40
41
42
43
44
45
46
47
48
49
50

- 1
2
3 (21) Li, J. J.; Xiao, S. Y.; Xu, Y. X.; Zuo, S.; Zha, Z. S.; Ke, W. D.; He, C. X.; Ge, Z. S. Smart
4 Asymmetric Vesicles with Triggered Availability of Inner Cell-Penetrating Shells for Specific
5 Intracellular Drug Delivery. *ACS Appl. Mater. Interfaces* **2017**, *9*, 17727-17735.
6
7
8
9
10 (22) Rahoui, N.; Jiang, B.; Taloub, N.; Huang, Y. D. Spatio-Temporal Control Strategy of Drug
11 Delivery Systems Based Nanostructures. *J. Controlled Release* **2017**, *255*, 176-201.
12
13
14 (23) Shanmugam, V.; Selvakumar, S.; Yeh, C.-S. Near-Infrared Light-Responsive
15 Nanomaterials in Cancer Therapeutics. *Chem. Soc. Rev.* **2014**, *43*, 6254-6287.
16
17
18
19 (24) Jia, S.; Fong, W. K.; Graham, B.; Boyd, B. J. Photoswitchable Molecules in Long-
20 Wavelength Light-Responsive Drug Delivery: From Molecular Design to Applications. *Chem.*
21 *Mater.* **2018**, *30*, 2873-2887.
22
23
24
25 (25) Yang, G.; Liu, J.; Wu, Y.; Feng, L.; Liu, Z. Near-Infrared-Light Responsive Nanoscale
26 Drug Delivery Systems for Cancer Treatment. *Coord. Chem. Rev.* **2016**, *320*, 100-117.
27
28
29
30 (26) Saneja, A.; Kumar, R.; Arora, D.; Kumar, S.; Panda, A. K.; Jaglan, S. Recent Advances in
31 Near-Infrared Light-Responsive Nanocarriers for Cancer Therapy. *Drug Discov. Today* **2018**, *23*,
32 1115-1125.
33
34
35
36 (27) Min, Y.; Li, J.; Liu, F.; Yeow, E. K.; Xing, B. Near-Infrared Light-Mediated
37 Photoactivation of a Platinum Antitumor Prodrug and Simultaneous Cellular Apoptosis Imaging
38 by Upconversion-Luminescent Nanoparticles. *Angew. Chem. Int. Ed.* **2014**, *53*, 1012-1016.
39
40
41
42 (28) Wang, X.; Liu, K.; Yang, G.; Cheng, L.; He, L.; Liu, Y.; Li, Y.; Guo, L.; Liu, Z. Near-
43 Infrared Light Triggered Photodynamic Therapy in Combination with Gene Therapy Using
44 Upconversion Nanoparticles for Effective Cancer Cell Killing. *Nanoscale* **2014**, *6*, 9198-9205.
45
46
47
48 (29) Wu, S.; Butt, H. J. Near-Infrared-Sensitive Materials Based on Upconverting
49 Nanoparticles. *Adv. Mater.* **2016**, *28*, 1208-1226.
50
51
52
53
54
55
56
57
58
59
60

- 1
2
3 (30) Castano, A. P.; Demidova, T. N.; Hamblin, M. R. Mechanisms in Photodynamic Therapy:
4 Part One—Photosensitizers, Photochemistry and Cellular Localization. *Photodiagn. Photodyn.*
5 **2004**, *1*, 279-293.
6
7
8
9
10 (31) Zhou, Z.; Song, J.; Nie, L.; Chen, X. Reactive Oxygen Species Generating Systems
11 Meeting Challenges of Photodynamic Cancer Therapy. *Chem. Soc. Rev.* **2016**, *45*, 6597-6626.
12
13
14 (32) Liu, L. H.; Qiu, W. X.; Li, B.; Zhang, C.; Sun, L. F.; Wan, S. S.; Rong, L.; Zhang, X. Z. A
15 Red Light Activatable Multifunctional Prodrug for Image Guided Photodynamic Therapy and
16 Cascaded Chemotherapy. *Adv. Funct. Mater.* **2016**, *26*, 6257-6269.
17
18
19 (33) Wilson, D. S.; Dalmasso, G.; Wang, L.; Sitaraman, S. V.; Merlin, D.; Murthy, N. Orally
20 Delivered Thioketal Nanoparticles Loaded with TNF- α -siRNA Target Inflammation and Inhibit
21 Gene Expression in the Intestines. *Nat. Mater.* **2010**, *9*, 923-928.
22
23
24 (34) Shim, M. S.; Xia, Y. A Reactive Oxygen Species (ROS)-Responsive Polymer for Safe,
25 Efficient, and Targeted Gene Delivery in Cancer Cells. *Angew. Chem. Int. Ed.* **2013**, *52*, 6926-
26 6929.
27
28
29 (35) Yue, C.; Yang, Y.; Zhang, C.; Alfranca, G.; Cheng, S.; Ma, L.; Liu, Y.; Zhi, X.; Ni, J.;
30 Jiang, W. ROS-Responsive Mitochondria-Targeting Blended Nanoparticles: Chemo-and
31 Photodynamic Synergistic Therapy for Lung Cancer with on-Demand Drug Release upon
32 Irradiation with a Single Light Source. *Theranostics* **2016**, *6*, 2352-2366.
33
34
35 (36) Xu, X.; Saw, P. E.; Tao, W.; Li, Y.; Ji, X.; Bhasin, S.; Liu, Y.; Ayyash, D.; Rasmussen, J.;
36 Huo, M. ROS-Responsive Polyprodrug Nanoparticles for Triggered Drug Delivery and Effective
37 Cancer Therapy. *Adv. Mater.* **2017**, *29*, 1700141. doi: 10.1002/adma.201700141
38
39
40 (37) Xu, Q.; He, C.; Xiao, C.; Chen, X. Reactive Oxygen Species (ROS) Responsive Polymers
41 for Biomedical Applications. *Macromol. Biosci.* **2016**, *16*, 635-646.
42
43
44
45
46
47
48
49
50
51
52
53
54
55
56
57
58
59
60

- 1
2
3 (38) Yuan, Y. Y.; Liu, J.; Liu, B. Conjugated-Polyelectrolyte-Based Polyprodrug: Targeted and
4 Image-Guided Photodynamic and Chemotherapy with On-Demand Drug Release upon
5
6 Irradiation with a Single Light Source. *Angew. Chem. Int. Ed.* **2014**, *53*, 7163-7168.
7
8
9
10 (39) Li, J.; Sun, C.; Tao, W.; Cao, Z.; Qian, H.; Yang, X.; Wang, J. Photoinduced PEG
11
12 Deshielding from ROS-Sensitive Linkage-Bridged Block Copolymer-Based Nanocarriers for on-
13
14 Demand Drug Delivery. *Biomaterials* **2018**, *170*, 147-155.
15
16
17 (40) Cao, Z.; Ma, Y.; Sun, C.; Lu, Z.; Yao, Z.; Wang, J.; Li, D.; Yuan, Y.; Yang, X. ROS-
18
19 Sensitive Polymeric Nanocarriers with Red Light-Activated Size Shrinkage for Remotely
20
21 Controlled Drug Release. *Chem. Mater.* **2018**, *30*, 517-525.
22
23
24 (41) Treat, N. J.; Smith, D.; Teng, C.; Flores, J. D.; Abel, B. A.; York, A. W.; Huang, F.;
25
26 McCormick, C. L. Guanidine-Containing Methacrylamide (Co) polymers via a RAFT: Toward a
27
28 Cell-Penetrating Peptide Mimic. *ACS Macro Lett.* **2011**, *1*, 100-104.
29
30
31 (42) Yin, W.; Ke, W.; Chen, W.; Xi, L.; Zhou, Q.; Mukerabigwi, J. F.; Ge, Z. Integrated Block
32
33 Copolymer Prodrug Nanoparticles for Combination of Tumor Oxidative Stress Amplification
34
35 and ROS-Responsive Drug Release. *Biomaterials* **2019**, *195*, 63-74.
36
37
38 (43) Semsarilar, M.; Ladmiral, V.; Blanazs, A.; Armes, S. Anionic Polyelectrolyte-Stabilized
39
40 Nanoparticles via RAFT Aqueous Dispersion Polymerization. *Langmuir* **2011**, *28*, 914-922.
41
42
43 (44) Huang, M.; Li, H.; Ke, W.; Li, J.; Zhao, C.; Ge, Z. Finely Tuned Thermo-Responsive Block
44
45 Copolymer Micelles for Photothermal Effect-Triggered Efficient Cellular Internalization.
46
47 *Macromol. Biosci.* **2016**, *16*, 1265-1272.
48
49
50 (45) Kruk, J.; Szymanska, R. Singlet Oxygen and Non-Photochemical Quenching Contribute to
51
52 Oxidation of the Plastoquinone-Pool Under High Light Stress in Arabidopsis. *BBA-Bioenergetics*
53
54 **2012**, *1817*, 705-710.
55
56
57
58
59
60

- 1
2
3 (46) Chou, T.-C. Theoretical Basis, Experimental Design, and Computerized Simulation of
4 Synergism and Antagonism in Drug Combination Studies. *Pharmacol. Rev.* **2006**, *58*, 621-681.
5
6
7 (47) Sun, C.-Y.; Cao, Z.; Zhang, X.-J.; Sun, R.; Yu, C.-S.; Yang, X. Cascade-Amplifying
8 Synergistic Effects of Chemo-Photodynamic Therapy Using ROS-Responsive Polymeric
9 Nanocarriers. *Theranostics* **2018**, *8*, 2939-2953.
10
11
12 (48) Han, K.; Lei, Q.; Wang, S. B.; Hu, J. J.; Qiu, W. X.; Zhu, J. Y.; Yin, W. N.; Luo, X.;
13 Zhang, X. Z. Dual-Stage-Light-Guided Tumor Inhibition by Mitochondria-Targeted
14 Photodynamic Therapy. *Adv. Funct. Mater.* **2015**, *25*, 2961-2971.
15
16
17 (49) Ashton, J. C. Drug Combination Studies and Their Synergy Quantification Using the
18 Chou–Talalay Method. *Cancer Res.* **2015**, *75*, 2400-2400.
19
20
21 (50) Saravanakumar, G.; Kim, J.; Kim, W. J. Reactive-Oxygen-Species-Responsive Drug
22 Delivery Systems: Promises and Challenges. *Adv. Sci.* **2017**, *4*. doi: 10.1002/advs.201600124.
23
24
25 (51) Ye, H.; Zhou, Y.; Liu, X.; Chen, Y. B.; Duan, S. Z.; Zhu, R. Y.; Liu, Y.; Yin, L. C. Recent
26 Advances on Reactive Oxygen Species-Responsive Delivery and Diagnosis System.
27 *Biomacromolecules* **2019**, *20*, 2441-2463.
28
29
30
31
32
33
34
35
36
37
38
39
40
41
42
43
44
45
46
47
48
49
50
51
52
53
54
55
56
57
58
59
60

For Table of Contents Only

